DMD Fast Forward. Published on December 28, 2018 as DOI: 10.1124/dmd.118.084194
This article has not been copyedited and formatted. The final version may differ from this version.

Hepatic OATP-mediated clearance in the Beagle dog: assessing in vitro-in vivo relationships and applying cross species empirical scaling factors to improve prediction of human clearance

Norikazu Matsunaga, Ayşe Ufuk, Bridget L. Morse, David W. Bedwell, Jingqi Bao, Michael A. Mohutsky, Kathleen M. Hillgren, Stephen D. Hall, J. Brian Houston, and Aleksandra Galetin

Centre for Applied Pharmacokinetic Research, University of Manchester, UK (N.M., A.U., J.B.H., and A.G.), Pharmacokinetic Research Laboratories, Ono Pharmaceutical Co., Ltd., Japan (N.M.), and Lilly Research Laboratories, Eli Lilly and Company, USA (B.L.M., D.W.B., J.B., M.A.M., K.M.H., and S.D.H.)

Downloaded from dmd.aspetjournals.org at ASPET Journals on April 17, 2024

DMD Fast Forward. Published on December 28, 2018 as DOI: 10.1124/dmd.118.084194
This article has not been copyedited and formatted. The final version may differ from this version.

Running title: Hepatic transporter-mediated clearance in beagle dogs

Corresponding author:

Dr Aleksandra Galetin

Centre for Applied Pharmacokinetic Research, School of Health Sciences, University of Manchester

Stopford building, Oxford Road, Manchester, M13 9PT, UK

Email address: Aleksandra.Galetin@manchester.ac.uk Telephone: +44 161 275 6886

Manuscript metrics:

Number of text page: 28

Number of tables: 4

Number of figures: 6

Number of references: 43

Number of words in the Abstract: 250

Number of words in the Introduction: 794

Number of words in the Discussion: 1542

Abbreviations:

ABT, 1-aminobenzotriazole; BSP, sulfobromophthalein, CL_{active}, active uptake clearance; $CL_{int,H}$, intrinsic hepatic clearance; $CL_{int,met}$, intrinsic metabolic clearance; $CL_{int,uptake}$, intrinsic uptake clearance; $CL_{passive}$, passive diffusion clearance; CL_{uptake}, total uptake clearance; fu_{cell}, fraction unbound in cells; DDI, drug-drug interaction; DPBS, Dulbecco's phosphate-buffered saline; fu_p, fraction unbound in plasma; gmfe, geometric fold error; IVIVE, in vitro-in vivo extrapolation; Kp, total cell-to-medium concentration ratio; Kp_{uu}, cell-to-medium concentration ratio for unbound drug; LC-MS/MS, liquid chromatography with tandem mass spectrometry; OATP/Oatp, organic anion transporting polypeptide; UGT, UDP-glucuronosyltransferase

Downloaded from dmd.aspetjournals.org at ASPET Journals on April 17, 2024

DMD Fast Forward. Published on December 28, 2018 as DOI: 10.1124/dmd.118.084194
This article has not been copyedited and formatted. The final version may differ from this version.

Abstract

In the present study the beagle dog was evaluated as a preclinical model to investigate organic anion transporting polypeptide (OATP)-mediated hepatic clearance. In vitro studies were performed with nine OATP substrates in three lots of plated male dog hepatocytes +/- OATP inhibitor cocktail to determine total uptake (CL_{uptake}), total and unbound cell-to-medium concentration ratio (Kp_{uu}). In vivo intrinsic hepatic clearances ($CL_{int,H}$) were determined following intravenous drug administration (0.1 mg/kg) in male beagle dogs. The in vitro parameters were compared to those previously reported in plated human, monkey and rat hepatocytes; the ability of cross species scaling factors to improve prediction of human in vivo clearance was assessed. CL_{uptake} in dog hepatocytes ranged from 9.4-135 µL/min/10^6cells for fexofenadine and telmisartan, respectively. Active process contributed >75% to CL_{uptake} for 5/9 drugs. Rosuvastatin and valsartan showed Kp_{uu}>10, whereas cerivastatin, pitavastatin, repaglinide and telmisartan had Kp_{uu}<5. The extent of hepatocellular binding in dog was consistent with other preclinical species and humans. The bias (2.73-fold) obtained from comparison of predicted *vs.* in vivo dog $CL_{int,H}$ was applied as an average empirical scaling factor (ESF_{av}) for in vitro-in vivo extrapolation of human $CL_{int,H}$. The ESF_{av} based on dog reduced under-prediction of human $CL_{int,H}$ for the same dataset (gmfe=2.1), highlighting its utility as a preclinical model to investigate OATP-mediated uptake. The $ESF_{av,}$ from all preclinical species resulted in comparable improvement of human clearance prediction, in contrast to drug specific empirical scalars, rationalized by species differences in expression and/or relative contribution of particular transporters to drug hepatic uptake.

Downloaded from dmd.aspetjournals.org at ASPET Journals on April 17, 2024

DMD Fast Forward. Published on December 28, 2018 as DOI: 10.1124/dmd.118.084194
This article has not been copyedited and formatted. The final version may differ from this version.

Introduction

For many acidic or zwitterionic drugs, transporter-mediated uptake clearance is an important contributor to hepatic disposition and can be a rate determining process for drug hepatic clearance and corresponding drug-drug interactions (DDIs) (Gertz et al., 2013; Shitara et al., 2013; Zamek-Gliszczynski et al., 2013; Varma et al., 2015). The value of in vitro derived transporter kinetic data within physiologically-based pharmacokinetic (PBPK) paradigm is now widely appreciated (Jones et al., 2015; Galetin et al., 2017; Yoshida et al., 2017; Guo et al., 2018), yet prediction success is still limited. Robust studies using preclinical animals to increase confidence in the subsequent application of in vitro-in vivo extrapolation (IVIVE) of human in vitro transporter data (De Bruyn et al., 2018) would help alleviate this shortcoming.

Recently, we demonstrated the utility of the cynomologus monkey as a preclinical species for evaluation of organic anion transporting polypeptide (OATP) mediated hepatic clearance and DDIs (De Bruyn et al., 2018; Ufuk et al., 2018). Despite overall good relationship between in vitro derived clearance in cynomologus monkey hepatocytes and in vivo clearance in same species, the under-prediction trend was apparent. The bias correction noted for the cynomologus monkey clearance prediction was subsequently applied as an empirical scaling factor (ESF) to improve the prediction of human hepatic clearance for the same OATP substrates from human hepatocytes. The success of the cross species scaling approach based on cynomologus monkey may be linked to the excellent agreement with human in OATP protein sequence homology. This work was extended to include two widely used preclinical species, the beagle dog and Sprague Dawley rat, for which OATP proteomics is less well defined, but believed to show poor homology with human.

An increasing number of studies have recently investigated hepatic uptake transporter-mediated clearance and DDIs in cynomolgus monkeys, both in vitro and in vivo (Shen et al., 2013; Chu et al., 2015; De Bruyn et al., 2018; Ufuk et al., 2018). In contrast, there is minimal information or systematic evaluation of activity of hepatic transporters in beagle dogs (Wilby et al., 2011). Studies in rat have been limited to hepatocyte investigations and predictions of in vivo clearance have been inconsistent (Huang et al., 2010;

Downloaded from dmd.aspetjournals.org at ASPET Journals on April 17, 2024

DMD Fast Forward. Published on December 28, 2018 as DOI: 10.1124/dmd.118.084194
This article has not been copyedited and formatted. The final version may differ from this version.

Wood et al., 2017). Recent protein quantification by mass spectrometry has revealed interspecies differences in absolute expression levels of hepatobiliary transporters in the liver and drug-metabolizing enzymes in various species (Heikkinen et al., 2015; Wang et al., 2015). Canine Oatp1b4 is the most abundant transporter and represents approximately a half of total abundance of hepatobiliary transporters in dog liver, in contrast to human OATP1B1 and OATP1B3 which contribute only approximately 29% to total abundance of hepatic transporters expressed in human liver (Wang et al., 2015). Oatp1a1, Oatp1a4, and Oatp1b2 are major Oatp transporters expressed on the sinusoidal membrane of rat hepatocytes (Wang et al., 2015). In cynomolgus monkeys, Oatp1b1 and Oatp1b3 are mainly expressed in the liver (Wang et al., 2015), showing high level of amino acid homology (>90%) between human and cynomolgus monkey transporter counterparts (Shen et al., 2013). In the case of beagle dogs, Oatp1b4 shows 68% and 71% homology at protein level to human OATP1B1 and OATP1B3, respectively (Gui and Hagenbuch, 2010).

To date, limited in vitro and in vivo data have been reported in the beagle dog for OATP-mediated hepatic clearances and examples of IVIVE of transporter-mediated hepatic clearance in this preclinical species are few. Here we report the in vitro characterization of hepatic uptake for 9 known OATP substrates namely, atorvastatin, cerivastatin, fexofenadine, pitavastatin, pravastatin, repaglinide, rosuvastatin, telmisartan, and valsartan in plated male dog hepatocytes +/- cocktail of OATP inhibitors. Based on data in other preclinical species and human, selected OATP substrates cover a range of low to high clearance drugs with different contribution of active vs. passive processes to the overall hepatic clearance. In addition to in vitro, in vivo pharmacokinetic studies were conducted in beagle dogs following intravenous drug administration in order to evaluate hepatic clearance prediction by IVIVE. The use of dog ESFs to refine prediction of human clearance was explored, as recently reported for data obtained in cynomolgus monkey hepatocytes (De Bruyn et al., 2018). Dataset average and individual drug specific ESFs (ESF_{av} and ESF_{sd}, respectively), derived from the relationship between in vivo and in vitro predicted clearance in beagle dog were determined. A similar exercise was performed for the rat using previously published hepatocyte kinetic data derived under similar experimental conditions (Ménochet et al., 2012a; Cantrill and Houston, 2017) to those reported here for the dog studies. Furthermore, in vitro derived parameters

Downloaded from dmd.aspetjournals.org at ASPET Journals on April 17, 2024

DMD Fast Forward. Published on December 28, 2018 as DOI: 10.1124/dmd.118.084194
This article has not been copyedited and formatted. The final version may differ from this version.

were compared across all preclinical species investigated. The extent of improvement in human clearance prediction based on application of ESFs from beagle dog was compared to the application of ESFs from monkey and rat data for the same dataset of OATP substrates.

Downloaded from dmd.aspetjournals.org at ASPET Journals on April 17, 2024

DMD Fast Forward. Published on December 28, 2018 as DOI: 10.1124/dmd.118.084194
This article has not been copyedited and formatted. The final version may differ from this version.

Material and Methods

Chemicals. 1-aminobenzotriazole (ABT), atorvastatin, fexofenadine, pravastatin, repaglinide, rifamycin SV, and sulfobromophthalein (BSP) were purchased from Sigma-Aldrich (Poole, UK). Atorvastatin lactone, repaglinide acyl-β-D-glucuronide, and telmisartan acyl-β-D-glucuronide were purchased from Toronto Research Chemicals Inc. (North York, Canada). Cerivastatin, Pitavastatin, rosuvastatin, and valsartan were purchased from Sequoia Research Products (Pangbourne, UK). For in vivo studies, atorvastatin, telmisartan and rosuvastatin were purchased from Thermo Fisher Scientific (New Jersey, USA). Pitavastatin and repaglinide were purchased from Selleck Chemicals (Houston, TX). Fexofenadine and pravastatin were purchased from TCI America (Portland, OR). Valsartan was purchased from Sigma Aldrich (St. Louis, MO). Cerivastatin was purchased from Ochem Incorporation (Des Plaines, IL).

Hepatocyte uptake studies. Cryopreserved male beagle dog hepatocytes (lots XVD, XZG, and YHF, all single donors) were purchased from BioIVT (Baltimore, MD). Cryopreserved dog hepatocytes were thawed according to manufacturer's standard protocol, and 0.5 mL of suspended hepatocytes (0.7×10^6 viable cells/mL) was added to each well of collagen I-coated BioCoat™ 24-well plates (BD Biosciences, Bedford, MA). After 4 h culturing in a CO_2 incubator, the medium was discarded, and the cell monolayers were pre-incubated with Dulbecco's phosphate-buffered saline (DPBS) containing 1 mM ABT +/- OATP inhibitor cocktail (100 µM rifamycin SV and 50 µM BSP) for 30 min. ABT was used as a pan-inhibitor to inactivate cytochrome P450 (CYP) activities in dog hepatocytes. Uptake data in the presence of OATP inhibitor cocktail were used to determine the $CL_{passive}$ value. This approach was based on preliminary data that showed more pronounced inhibition of uptake of prototypical OATP probes pitavastatin and repaglinide in dog hepatocytes compared to the use of rifamycin SV or BSP alone (data not shown). Subsequently, uptake was started by adding fresh DPBS containing OATP substrate at a concentration of 0.5 µM with the exception of pravastatin (5 µM) +/- OATP inhibitor cocktail over 2 min at 37°C. The buffer was collected and 200 µL of water was added to lyse the cells after washing the cells with ice-cooled DPBS three times. All uptake experiments were performed in triplicate. In addition, extended uptake studies over 90 min (with up to 8 time points) were performed in order to reach equilibrium and determine the total cell-to-medium drug concentration ratio (Kp); the same low drug concentration was used as in

Downloaded from dmd.aspetjournals.org at ASPET Journals on April 17, 2024

DMD Fast Forward. Published on December 28, 2018 as DOI: 10.1124/dmd.118.084194
This article has not been copyedited and formatted. The final version may differ from this version.

shorter incubations. Any potential cell loss was accounted for by measuring protein concentrations in cell lysates using the bicinchoninic acid (BCA) assay according to manufacturer's protocol (Life Technologies Ltd., Paisley, UK). Drug concentrations in cell lysate and medium were quantified by liquid chromatography with tandem mass spectrometry (LC-MS/MS); conditions are detailed in the Supplemental Table S1. In addition, the metabolism of atorvastatin to atorvastatin lactone (Prueksaritanont et al., 2002) and repaglinide and telmisartan to their respective acyl-glucuronides (Gill et al., 2012; Sall et al., 2012) was monitored.

Determination of plasma protein binding. Fraction unbound in dog plasma (fu_p) was determined for all compounds via equilibrium dialysis at a concentration of 1 µM. Briefly, pre-soaked dialysis membranes were placed in a 96-well microequilibrium dialysis device, then 125 µL of plasma spiked with compound was loaded opposite to 100 µL of 100 mM sodium phosphate buffer (pH 7.4) in triplicate. Plates were sealed and incubated at 37°C with 5% CO_2 for 4 h, shaking at 200 rpm, after which 25 µL of plasma/buffer was taken and mixed with 25 µL buffer/plasma. The 50 µL samples were then quenched with 150 µL acetonitirile containing internal standard for the individual compound and concentrations quantified via LC-MS/MS, as described in Supplemental Table S2. Recovery over the 4 h period was tested for all compounds and ranged from 97-108%.

In vivo studies. In vivo study protocol was reviewed and approved by the Institutional Animal Care and Use Committee. Male beagle dogs (n=3 / study arm) weighed 8-15 kg at the time of study conduct and were fasted overnight prior to being administered compound. All compounds were intravenously administered at 0.1 mg/kg as a 20% captisol solution and were given over 30 min via a temporary catheter inserted into the cephalic vein. Blood samples were taken from the jugular vein at 0.25, 0.42, 0.58, 0.75, 1, 1.5, 2.5, 4.5, 8.5, 12.5 and 24.5 h following administration. Blood samples were collected in tubes containing EDTA and centrifuged to collect plasma. Studies were carried out in cages with plexiglass surroundings for collection of urine from 0-4, 4-8, 8-12, and 12-24 h. Additional blood samples were taken at pre-dose, 4, 8, 12, and 24 h for measurement of plasma creatinine. Creatinine was also measured in an aliquot from each urine collection interval. Plasma and urine samples for determination of

Downloaded from dmd.aspetjournals.org at ASPET Journals on April 17, 2024

DMD Fast Forward. Published on December 28, 2018 as DOI: 10.1124/dmd.118.084194
This article has not been copyedited and formatted. The final version may differ from this version.

compound concentrations were stored at ≤-20℃ until analysis via LC-MS/MS, as described in Supplemental Table S2.

Analysis of In Vitro Hepatocyte Data. In vitro uptake rates (pmol/min/mg protein) were calculated from the slopes of the initial uptake rate-time profile in the absence and presence of OATP inhibitor cocktail; the rates were then divided by the initial substrate concentration to determine total uptake clearance (CL_{uptake}, μL/min/mg protein) and passive diffusion clearance ($CL_{passive}$, μL/min/mg protein), respectively (Yabe et al., 2011). Passive influx diffusion clearance was assumed to be equal to the passive efflux and effect of membrane potential (Yoshikado et al., 2017) was not considered. Adsorption of the drug to the plate in the absence of cells was <7% across all substrates investigated, regardless of the presence of OATP inhibitor cocktail. In vitro hepatic active uptake clearance (CL_{active}) was calculated by subtracting the $CL_{passive}$ from the CL_{uptake} (Yabe et al., 2011). The conversion of CL_{uptake}, $CL_{passive}$, and CL_{active} to μL/min/10^6cells was carried out using 1.2 mg protein/10^6 dog hepatocytes based on in-house data generated using the BCA assay (not shown). The $CL_{passive}$ was log-transformed and compared with the $logD_{7.4}$ values of the drugs investigated taken from a previous study (Yabe et al., 2011). The Kp parameter, which represents intracellular binding in addition to active uptake processes, was calculated from eq. 1:

$$Kp = C_{cell}/C_{medium} \qquad (1)$$

where, C_{cell} and C_{medium} represent drug concentrations in cells and medium, respectively. The hepatocyte volume was set to 3.9 μL per 10^6 hepatocytes with an assumption of the same volume as reported in rat (Reinoso et al., 2001). The cell-to-medium concentration ratio for unbound drug (Kp_{uu}) was calculated from eq. 2 (Yabe et al., 2011; Shitara et al., 2013):

$$Kp_{uu} = CL_{uptake}/\left(CL_{passive} + CL_{int}\right) \qquad (2)$$

where, CL_{int} represents intrinsic clearance for either metabolism and/or biliary excretion. Cerivastatin, fexofenadine, pitavastatin, pravastatin, rosuvastatin and valsartan are metabolically stable or metabolized mainly by CYP. Metabolic clearance was assumed negligible for these drugs because ABT, a pan CYP inhibitor, was included in the incubations. The biliary excretion of all the drugs investigated was considered negligible under the current experimental set up due to internalization of transporters following

Downloaded from dmd.aspetjournals.org at ASPET Journals on April 17, 2024

DMD Fast Forward. Published on December 28, 2018 as DOI: 10.1124/dmd.118.084194
This article has not been copyedited and formatted. The final version may differ from this version.

short-term culturing (Bow et al., 2008). The formation of atorvastatin lactone, repaglinide and telmisartan glucuronides was not negligible under prolonged incubation times used to determine the Kp. Therefore, intrinsic metabolic clearance ($CL_{int,met}$) was calculated from the slope of the linear phase of metabolite formation over time and these $CL_{int,met}$ values were used to calculate Kp_{uu} of atorvastatin, repaglinide, and telmisartan using eq. 2. The fraction unbound in the cell (fu_{cell}) was calculated using eq. 3 (Yabe et al., 2011):

$$fu_{cell} = Kp_{uu}/Kp \qquad (3)$$

In addition to the analysis of the initial uptake rate data, the fu_{cell}, CL_{active} and $CL_{passive}$ were determined by simultaneous fitting of uptake data over an extended time course in the absence and presence of OATP inhibitor cocktail. An adaptation of the mechanistic two-compartment model (Ménochet et al., 2012b) in MATLAB (version 8.5.1, 2015; Mathworks, Natick, MA) was applied to estimate CL_{active}, $CL_{passive}$ and fu_{cell} under the assumption that CL_{active} in eqs. 4 and 5 approaches zero in the presence of transporter inhibitors. As a proof of concept, this method was only applied for 6 drugs that do not undergo metabolism under the experimental conditions employed (cerivastatin, fexofenadine, pitavastatin, pravastatin, rosuvastatin, and valsartan) and using lot XVD of dog hepatocytes.

$$\frac{dS_{cell}}{dt} = \frac{(CL_{active} + CL_{passive}) \times S_{med} - CL_{passive} \times S_{cell} \times fu_{cell}}{V_{cell}} \qquad (4)$$

$$\frac{dS_{med}}{dt} = \frac{-(CL_{active} + CL_{passive}) \times S_{med} + CL_{passive} \times S_{cell} \times fu_{cell}}{V_{med}} \qquad (5)$$

where, S_{cell} and S_{med} represent the intracellular and media drug concentrations, respectively. V_{cell} and V_{med} are the intracellular and medium volumes which were set at 3.9 µL and 400 µL, respectively.

Analysis of In Vivo Dog Data. In vivo data were analyzed using Watson LIMS 7.5 (Thermo Fisher). Systemic in vivo plasma clearance (CL_{total}) was determined using eq. 6:

$$CL_{total} = \frac{Dose}{AUC_{0-\infty}} \qquad (6)$$

where $AUC_{0-\infty}$ represents the extrapolated area under the plasma concentration-time curve. For compounds with measurable urinary excretion, renal clearance (CL_R) was determined with eq. 7;

Downloaded from dmd.aspetjournals.org at ASPET Journals on April 17, 2024

DMD Fast Forward. Published on December 28, 2018 as DOI: 10.1124/dmd.118.084194
This article has not been copyedited and formatted. The final version may differ from this version.

$$CL_R = \frac{Ae_{0-24}}{AUC_{0-24}} \qquad (7)$$

where $Ae_{0\text{-}24}$ and $AUC_{0\text{-}24}$ represent the amount excreted in the urine and the area under the plasma concentration-time curve from 0-24 hours, respectively. To account for possible incomplete urine collection, CL_R was corrected for recovery of creatinine in the urine. CL_R for creatinine was calculated as shown in eq. 7 and corrected CL_R for drugs investigated was obtained as shown in eq. 8:

$$corrected\ CL_R = CL_R \div \frac{creatinineCL_R}{GFR} \qquad (8)$$

where GFR represents reported glomerular filtration rate in dogs of 3.2 mL/min/kg (Mahmood, 1998).
In addition to creatinine, plasma iohexol clearance was measured and values obtained were comparable to creatinine clearance (data not shown). In vivo hepatic clearance (CL_H) was calculated by subtracting CL_R from CL_{total}.

Extrapolation of in vitro hepatic uptake clearance to in vivo. The IVIVE method was based on the overall uptake clearance parameter and therefore net effect of multiple processes is captured. Dog in vitro CL_{uptake} (µL/min/10^6cells) was scaled by a hepatocellularity value of 175 × 10^6 cells/g liver and average dog liver weight of 32 g liver/body weight. A median value of hepatocellularity values reported in the literature for beagle dogs was used (details of data collation in Supplemental Table S3). In vivo $CL_{int,H}$ (mL/min/kg) was obtained applying the well-stirred model (eq. 9):

$$CL_{int,H} = \frac{CL_H}{\frac{f_u}{R_b} \times (1 - \frac{CL_H}{Q_h})} \qquad (9)$$

where, Q_H represents average hepatic blood flow in beagle dog of 40 mL/min/kg (summary of individual studies reported in the literature is in the Supplemental Table S3) and R_B represents blood-to-plasma ratio. For atorvastatin, the CL_H corrected by R_B value was greater than Q_H, therefore, the blood-based $CL_{H,B}$ (CL_H/R_B) value was capped at 90% of canine hepatic blood flow (36 mL/min/kg). Differences in $CL_{int,H}$ predicted from in vitro data relative to in vivo $CL_{int,H}$ and the corresponding precision of the prediction were assessed by geometric mean fold error (gmfe, eq. 10) and the root mean squared error (rmse, eq. 11) (Gertz et al., 2010), respectively:

Downloaded from dmd.aspetjournals.org at ASPET Journals on April 17, 2024

DMD Fast Forward. Published on December 28, 2018 as DOI: 10.1124/dmd.118.084194
This article has not been copyedited and formatted. The final version may differ from this version.

$$gmfe = 10^{\frac{1}{N}\Sigma\left|log\left(\frac{predicted\ CL_{int,H}}{observed\ CL_{int,H}}\right)\right|} \quad (10)$$

$$rmse = \sqrt{\frac{1}{N}\sum(predicted - observed)^2} \quad (11)$$

where N indicates the number of drugs included in analysis.

To evaluate whether dog as a preclinical species can improve prediction of hepatic uptake transporter-mediated clearance in humans, the gmfe obtained from dog IVIVE was applied as an ESF_{av} in human predictions. In addition to ESF_{av}, the performance of human clearance prediction was assessed by using drug specific ESF obtained from the ratio of observed to predicted clearance in dog for each individual drug (ESF_{sd}) (Naritomi et al., 2001; Ito and Houston, 2005; De Bruyn et al., 2018). In addition to dog, the same strategy was applied using scalars obtained from the IVIVE of monkey and rat in vitro data obtained in plated hepatocytes and for the same set of OATP substrates. For monkey, the ESF values were taken from the previous publication (De Bruyn et al., 2018). In the case of rat, the ESFs were calculated from previously reported in vitro data in rat hepatocytes (Ménochet et al., 2012a; Cantrill and Houston, 2017) and literature collated in vivo clearance values (details listed in Supplemental Table S4). The direct IVIVE of human clearance was performed using the mean of in vitro data from four donors of human hepatocytes for which OATP1B1 c.521T>C genotype information was not known (Ménochet et al., 2012b; De Bruyn et al., 2018). Considering variability in transporter expression and/or activity in different lots of human hepatocytes, in vitro data from multiple donors were included in the evaluation. To assess the ability of preclinical species to refine prediction of human $CL_{int,H}$, the predicted $CL_{int,H}$ in humans for 9 OATP substrates were multiplied by either ESF_{av} or ESF_{sd} obtained from rat, dog (excluding bosentan as data were not available) and monkey.

Downloaded from dmd.aspetjournals.org at ASPET Journals on April 17, 2024

DMD Fast Forward. Published on December 28, 2018 as DOI: 10.1124/dmd.118.084194
This article has not been copyedited and formatted. The final version may differ from this version.

Results

Uptake parameters in dog hepatocytes. A time-dependent increase in intracellular accumulation was observed for all the nine drugs investigated. The mean uptake parameters obtained for individual drugs in three lots of dog hepatocytes are listed in Table 1; parameters obtained in each individual lot are summarized in Supplemental Table S5. A 15-fold range in CL_{uptake} was observed with cerivastatin showing the highest CL_{uptake} (143 ± 57 µL/min/10^6cells), followed by repaglinide, telmisartan, pitavastatin, and atorvastatin (CL_{uptake} >100 µL/min/10^6cells). In contrast, uptake was more than 10-fold lower in the case of fexofenadine and pravastatin (CL_{uptake} <10 µL/min/10^6cells). Drugs in the current dataset showed a 35-fold range in $CL_{passive}$; cerivastatin and pravastatin showed the highest and the lowest $CL_{passive}$, respectively. The formation of non-CYP metabolites was minimal over short incubation time and rates of metabolism represented 0.4%, 6.6%, and 9.9% of uptake rates of parent drugs for atorvastatin lactone, repaglinide glucuronide and telmisartan glucuronide, respectively. Therefore, $CL_{int,met}$ was not accounted for the calculation of CL_{active}. Overall, OATP substrates investigated in the current study showed >65% contribution of the active transport to total uptake, with 5/9 drugs having >75% of active contribution (Table 1). The CL_{active} values of pitavastatin, pravastatin, rosuvastatin, and valsartan were previously reported using freshly isolated male dog hepatocytes in suspension with temperature method (37℃ vs 4℃) (Wilby et al., 2011). Their CL_{active} values were similar to those obtained in the present study, suggesting only a marginal effect of cryopreservation and plated format on hepatic uptake transporter activities in dog hepatocytes despite difference in donors. Comparison of the CL_{uptake}, $CL_{passive}$, and CL_{active} values obtained in the individual donors of dog hepatocytes resulted in the overall good agreement (Supplemental Table S5), with most of the parameter values within 2-fold between individual donors with the exception of fexofenadine where CL_{uptake}, $CL_{passive}$, and CL_{active} showed differences across donors resulting in large CV on those parameters (58-93%). In addition to fexofenadine, pravastatin $CL_{passive}$ showed more than 3-fold difference among donors.

The in vitro uptake parameters of 8 drugs (cerivastatin, fexofenadine, pravastatin, pitavastatin, repaglinide, rosuvastatin, telmisartan, and valsartan) in dog hepatocytes were compared with those reported in human hepatocytes under similar experimental conditions (De Bruyn et al., 2018) (Fig. 1). In each case

Downloaded from dmd.aspetjournals.org at ASPET Journals on April 17, 2024

DMD Fast Forward. Published on December 28, 2018 as DOI: 10.1124/dmd.118.084194
This article has not been copyedited and formatted. The final version may differ from this version.

comparison was made between scaled parameters (expressed per g liver) due to differences in hepatocellularity between dog and human. The CL_{uptake} values obtained in dog hepatocytes were in good agreement with values in human hepatocytes, whereas the correlation of the $CL_{passive}$ and CL_{active} values was less marked. Cerivastatin and telmisartan $CL_{passive}$ in human hepatocytes were approximately 3-fold greater than values obtained in dog hepatocytes, whereas opposite trends were seen for pravastatin and valsartan (Table 1). In the case of CL_{active}, values for pravastatin, cerivastatin, fexofenadine and valsartan were approximately 2 to 5-fold greater in dog hepatocytes.

Kp parameters in dog hepatocytes. The Kp profiles over 90 min were investigated for all the 9 drugs in three donors of plated dog hepatocytes. Most of the drugs investigated reached steady-state within 30 min except for fexofenadine and valsartan (Fig. S1). The mean Kp parameters from 3 lots are shown in Table 2 and values obtained in each individual lot are summarized in Supplemental Table S6. A 28-fold range in mean Kp values was observed for the current dataset, with values ranging from 13.6 ± 2.4 (pravastatin) to 375 ± 117 (atorvastatin). For 6 out of 9 drugs the Kp were >100, with the exception of rosuvastatin, fexofenadine and pravastatin. Analogous to the trends in uptake parameters, an overall good agreement was seen in Kp values obtained in different donors (within 3-fold difference); fexofenadine and pravastatin were again the outliers (Table S6).

UGT-mediated $CL_{int,met}$ values of atorvastatin, repaglinide, and telmisartan determined in the extended Kp experiments were at least 15% of their respective $CL_{passive}$ values. Therefore, the $CL_{int,met}$ was considered when calculating the Kp_{uu} for these 3 drugs (eq. 2). A 16-fold range was observed in Kp_{uu} values among 9 drugs. The Kp_{uu} of rosuvastatin and valsartan were >10, whereas cerivastatin, pitavastatin, repaglinide, and telmisartan showed Kp_{uu}<5. There was a large range in fu_{cell} (122-fold) in dog hepatocytes; high intracellular binding was observed for atorvastatin, cerivastatin, pitavastatin, repaglinide, and telmisartan (fu_{cell} <0.05). In addition, CL_{active}, $CL_{passive}$, and fu_{cell} for 6 drugs were estimated by simultaneous fitting of uptake data (single low drug concentration) over an extended time course +/- OATP inhibitor cocktail. The estimates obtained by the mechanistic two-compartment model (Table S7) were comparable to those calculated in the two-step analysis of data from short incubation and Kp experiments. The fitting of the mechanistic model to drug cell concentrations vs. time (+/- inhibitor), as well as goodness-of-fit plots, are

Downloaded from dmd.aspetjournals.org at ASPET Journals on April 17, 2024

DMD Fast Forward. Published on December 28, 2018 as DOI: 10.1124/dmd.118.084194
This article has not been copyedited and formatted. The final version may differ from this version.

illustrated for rosuvastatin as a representative drug in Fig. S2. The $CL_{passive}$ and fu_{cell} values for the 9 drugs investigated was strongly correlated with the respective $logD_{7.4}$ (Fig. S3A and B); a relationship was also noted between the extent of intracellular binding in dog hepatocytes and fu_p for the drugs investigated (Fig. S3C).

Species differences in uptake parameters. The CL_{uptake}, $CL_{passive}$ and CL_{active} in dog hepatocytes were compared with the previously reported values in Sprague Dawley rat, cynomolgus monkey and human (Ménochet et al., 2012b; Ménochet et al., 2012a; Cantrill and Houston, 2017; De Bruyn et al., 2018) (Fig. 2). Rat hepatocyte CL_{uptake} and CL_{active} values were generally in good agreement to those obtained in dogs, with rosuvastatin being an outlier in both cases (Fig. 2A and E). Rat hepatocyte $CL_{passive}$ values were similar to those in dog hepatocytes for cerivastatin, rosuvastatin and telmisartan, but were up to 6-fold smaller for the remaining drugs (Fig. 2C). Monkey hepatocyte total CL_{uptake} data showed a good agreement to dog hepatocytes data (Fig. 2B). In contrast to rat, $CL_{passive}$ values obtained in monkey hepatocytes were either similar to data in dog (fexofenadine, pitavastatin and pravastatin) or up to almost 6-fold greater for the remaining drugs (Fig. 2D). An opposite trend was seen for CL_{active} in which data were either comparable between the two species (rosuvastatin, telmisartan and valsartan), or up to approximately 6-fold smaller for the remaining drugs in monkey hepatocytes (Fig. 2F).

In vivo studies and extrapolation of dog in vitro transporter data to in vivo. The pharmacokinetic studies for the 9 drugs investigated were conducted following a single intravenous infusion over 30 min to three male beagle dogs. The in vivo parameters obtained are shown in Table 3. The CL_{total} values ranged from 1.48 ± 0.47 mL/min/kg (repaglinide) to 48.4 ± 13.3 mL/min/kg (atorvastatin). Hepatic clearance was the major elimination mechanism in beagle dog for the drugs investigated, as CL_R contributed <40 % to the CL_{total}. Five drugs (cerivastatin, fexofenadine, pitavastatin, pravastatin, repaglinide, and valsartan) were classified as low clearance drugs in beagle dogs, as their hepatic blood clearance ($CL_{H,B}$) was <30% of hepatic blood flow.

Downloaded from dmd.aspetjournals.org at ASPET Journals on April 17, 2024

DMD Fast Forward. Published on December 28, 2018 as DOI: 10.1124/dmd.118.084194
This article has not been copyedited and formatted. The final version may differ from this version.

The prediction of hepatic clearance in the dog is shown in Fig. 3. Good agreement between predicted and observed $CL_{int,H}$ was observed with a gmfe of 2.73 and 55% of values predicted within 2-fold of the observed data. Subsequently, the gmfe obtained in dog IVIVE for this dataset was applied to human IVIVE as an ESF_{av} with the aim to assess whether information obtained in dog as a preclinical species can improve prediction of hepatic uptake transporter-mediated clearance in humans. In addition to dog, a similar exercise was carried out using ESF_{av} obtained from IVIVE of rat and monkey in vitro data obtained for the same set of OATP substrates (Table 4). The in vitro and in vivo data of 9 drugs investigated in rat, monkey, and human are summarized in Supplemental Table S4, S8 and S9, respectively.

The direct prediction of human clearance from in vitro data (no ESF) resulted in under-prediction of in vivo $CL_{int,H}$ (3.22-fold bias, Table 4, Fig. 4). The improvement in prediction of human $CL_{int,H}$ observed using ESF_{av} was comparable across the three preclinical species, resulting in approximately 2-fold bias and increased precision (Table 4, Fig. 5A, C and E). This lack of difference in the prediction success between ESF_{av} from the three preclinical species is also reflected in the residual plots (Fig. 4C, Fig. 6). In contrast, the use of individual drug specific scaling factors (ESF_{sd}) resulted in species selective effects on the predictive performance (Fig. 4D). There was no improvement in the prediction bias of human clearance using rat ESF_{sd} (gmfe 3.41), with <25% of the drugs falling within the 2-fold error (Table 4, Fig. 5D). Use of ESF_{sd} obtained from dog and monkey data resulted in comparable bias (3.23- and 2.96-fold, respectively) with minor improvement in human clearance prediction. Higher proportion of drugs predicted within the 2-fold error was evident when monkey ESF_{sd} was applied (67%) relative to dog ESF_{sd} (25%) (Table 4, Fig. 5B and 5F, Fig. 6).

Species differences in Kp parameters. Large interspecies differences were apparent between Kp and Kp_{uu} (rank order of rat >dog >monkey seen for both parameters) (Fig. 7). Rat hepatocyte Kp and Kp_{uu} values were up to 23- and 7.4-fold larger than those in dog hepatocytes, respectively (Fig. 7A and D). The exceptions were repaglinide, telmisartan and valsartan Kp, and cerivastatin and fexofenadine Kp_{uu} which were comparable between the two species. In contrast, dog Kp and Kp_{uu} were comparable or greater than the data obtained in monkey hepatocytes with the exception of telmisartan Kp_{uu} (Fig. 7B and E).

Downloaded from dmd.aspetjournals.org at ASPET Journals on April 17, 2024

DMD Fast Forward. Published on December 28, 2018 as DOI: 10.1124/dmd.118.084194
This article has not been copyedited and formatted. The final version may differ from this version.

Differences in fexofenadine, pravastatin and valsartan were particularly marked, as dog Kp parameters were up to 6.2- greater than values obtained in monkey. The overall trends seen between dog and monkey Kp parameters were evident also in the comparison of dog and human Kp and Kp_{uu}, with the exception of valsartan. Even though Kp and Kp_{uu} showed species-dependent values, there was a good agreement in intracellular binding parameter across species. This trend was particularly strong between dog and monkey fu_{cell} data (1.76-fold bias), whereas 2.3- and 2.6-fold difference was seen in dog fu_{cell} relative to rat and human data, respectively.

Downloaded from dmd.aspetjournals.org at ASPET Journals on April 17, 2024

DMD Fast Forward. Published on December 28, 2018 as DOI: 10.1124/dmd.118.084194
This article has not been copyedited and formatted. The final version may differ from this version.

Discussion

The utility of the cynomologus monkey as a preclinical species for OATP-mediated hepatic clearance has recently been demonstrated and a good relationship between in vitro derived clearance in hepatocytes and in vivo clearance was observed (De Bruyn et al., 2018). As reported for metabolism related hepatic clearance predictions from hepatocytes (and other in vitro systems), under-prediction of transporter-mediated clearance also requires a bias correction to bridge the gap between extrapolated and observed values. This approach, applied retrospectively, is regarded as empirical and hence has no mechanistic basis. Recently, application of the bias correction observed in the IVIVE of cynomologus monkey clearance improved the prediction of human hepatic clearance for the same OATP substrates from human hepatocytes. Therefore, an analogous approach was applied here to two widely used preclinical species, beagle dog and Sprague Dawley rat. As a non-rodent preclinical species, beagle dogs are often used in pharmacokinetic studies; however, there is less information available to assess the predictive performance of hepatic transporter-mediated clearance and DDIs in this species compared to studies reported in cynomolgus monkeys (Shen et al., 2013; Chu et al., 2015; Watanabe et al., 2015; Ufuk et al., 2018). Therefore, characteristics of the hepatic uptake of a series of 9 drugs were investigated to provide a dataset of parameters for comparative purposes and evaluate beagle dogs as a preclinical animal model to study hepatic uptake.

In the present study, an OATP inhibitor cocktail was used to determine the $CL_{passive}$ value in dog hepatocytes. Substrate-dependent inhibition has been reported for human OATP1B1, OATP1B3, and OATP2B1 (Noe et al., 2007; Izumi et al., 2015; Barnett et al., 2018), and rationalized by multiple binding sites for substrates and inhibitors of OATP transporters. Accordingly, this may also be the case for canine Oatp1b4 and the use of multiple inhibitors for OATPs is preferable to determine the involvement of OATPs in hepatic uptake. Contributions of active uptake obtained here in dog hepatocytes (Table 1) were in good agreement with estimates previously reported in human hepatocytes (Ménochet et al., 2012b), suggesting minimal difference in active uptake contribution to cellular uptake between humans and dogs for OATP substrates. Some interspecies differences in $CL_{passive}$ values were apparent with up to 2.5-fold bias on average and an overall rank order of human ≥monkey >dog >rat. These differences may be

Downloaded from dmd.aspetjournals.org at ASPET Journals on April 17, 2024

DMD Fast Forward. Published on December 28, 2018 as DOI: 10.1124/dmd.118.084194
This article has not been copyedited and formatted. The final version may differ from this version.

attributed to incomplete inhibition of active uptake in some species and/or the differences in the methodologies used to estimate this parameter (e.g., use of a single inhibitor (monkey and human), cocktail of inhibitors (dog) and mechanistic modelling (rat)). However, for each species there was a good relationship with log $D_{7.4}$, consistent with other reports based on data obtained in transfected cell lines (Li et al., 2014).

Determining the extent of intracellular binding of drug in hepatocytes has important implications on understanding pharmacokinetic/pharmacodynamic relationships, drug efficacy and/or prediction of DDI risk (Zamek-Gliszczynski et al., 2013; Morse et al., 2015). Several experimental methods and in silico approaches to estimate intracellular drug concentration have been proposed (Chu et al., 2013; Guo et al., 2018), including the kinetic modeling used here. The fu_{cell} and $CL_{passive}$ values obtained in plated dog hepatocytes for 9 OATP substrates were strongly correlated with their $logD_{7.4}$ (Fig. S2), consistent with previous studies in both suspended and plated rat hepatocytes (Yabe et al., 2011; Ménochet et al., 2012a), as well as plated monkey and human hepatocytes (De Bruyn et al., 2018). This trend is expected as fu_{cell} is inversely related to Kp when no active transport occurs. Estimation of hepatic fu_{cell} from the correlation to $logD_{7.4}$ is well established and applicable for acidic compounds (Ménochet et al., 2012a; Chu et al., 2013) and provides a useful initial estimate of fu_{cell} in the case of limited data for implementation in the PBPK models. In addition, the current study showed promising approach of simultaneous fitting of total uptake data +/- OATP inhibitors over longer time period (up to steady-state) using a single low drug concentration which yielded comparable fu_{cell} estimates to indirect two-step method of the estimation of this parameter via Kp and Kp_{uu}.

Large interspecies differences were apparent in both Kp and Kp_{uu} values, with the general rank order of rat>dog>cynomolgus monkey ≈ human for drugs investigated (Fig. 7A to F). Kp_{uu} trends are not surprising as this parameter reflects interplay of active uptake and passive diffusion in addition to elimination processes (metabolism and biliary excretion). Interspecies differences in hepatic uptake clearance have been reported (Ménochet et al., 2012b; Watanabe et al., 2015), and correspond to some extent to differences in protein homology, but also to differences in absolute abundances of OATP/Oatp isoforms

Downloaded from dmd.aspetjournals.org at ASPET Journals on April 17, 2024

DMD Fast Forward. Published on December 28, 2018 as DOI: 10.1124/dmd.118.084194
This article has not been copyedited and formatted. The final version may differ from this version.

across species (Wang et al., 2015). Cynomolgus monkeys show 6- and 13-fold higher protein expressions of Oatp1b1 and Oatp1b3 compared with those in human OATP1B1 and OATP1B3, respectively, whereas comparable abundance is observed between dog Oatp1b4 and monkey Oatp1b1/Oatp1b3. In addition, the protein levels of rat Oatp1a1, Oatp1a4, and Oatp1b2 are lower than dog and monkey Oatps. In terms of the level of total protein (all OATP isoforms combined), the rank order is monkey >rat ≅dog >human (Wang et al., 2015). Comparison of CL_{active} across species (Fig. 2E and F) suggests that the interspecies differences of Kp_{uu} cannot be explained solely by protein expression levels of OATP/Oatp in the liver and that the interspecies differences in intrinsic transport affinity and capacity need to be also considered. Despite the discordance in Kp and Kp_{uu} of drugs between hepatocytes from dog and other species, there was a good agreement in intracellular binding parameter fu_{cell} between dog, monkey, rat and human (Fig. 7G and H). These findings are in agreement with recent reports on correlations of fu_{cell} or fu_{liver} between species for a diverse range of compounds (De Bruyn et al., 2018; Riccardi et al., 2018) and in relationships with $logD_{7.4}$ as a species-independent parameter.

A 33-fold range was observed in CL_H values in dog following a single intravenous infusion of 9 drugs investigated; the CL_{total} or CL_H values obtained in the present study were consistent with previous reports (pitavastatin CL_H, 6.8 mL/min/kg; pravastatin CL_H, 9.0 mL/min/kg; telmisartan CL_{total}, 6.75 mL/min/kg); valsartan CL_H, 8.3 mL/min/kg) (Deguchi et al., 2011; Wilby et al., 2011). In vitro prediction in dogs resulted in a good agreement with in vivo values with a 2.73-fold bias, and the predicted $CL_{int,H}$ values of 5/9 drugs investigated within 2-fold of in vivo $CL_{int,H}$ (Fig. 4). This average dog scaling factor improved human IVIVE performance by reducing the prediction bias (to 2.11-fold) and increasing precision. Use of ESF_{av} from other species resulted in a similar prediction success (2-fold bias in human IVIVE when using monkey and rat ESF_{av}). In contrast, use of ESF_{sd} resulted in a mixed success. Application of monkey ESF_{sd} for human prediction resulted in prediction bias of <3-fold with 67% of drugs predicted within 2-fold of the in vivo $CL_{int,H}$ values. In contrast, both the prediction accuracy and the proportion of drugs within the same error threshold were lower using dog and rat drug specific scalars (Table 4, Fig. 4 and 5). Although relatively smaller differences in drug specific scaling factors (observed to predicted $CL_{int,H}$ ratio) were observed between the species for a number of drugs (e.g., within 2.5-fold for repaglinide, telmisartan and

Downloaded from dmd.aspetjournals.org at ASPET Journals on April 17, 2024

DMD Fast Forward. Published on December 28, 2018 as DOI: 10.1124/dmd.118.084194
This article has not been copyedited and formatted. The final version may differ from this version.

pitavastatin), the differences in ESF_{sd} were more pronounced for pravastatin and cerivastatin (up to 27- and 4.6-fold larger in monkey and rat relative to the value obtained in dog, respectively). The present findings are based on a relatively small dataset of well-established OATP substrates; further studies with a larger number of transporter substrates, in particular with more challenging low clearance OATP drugs and/or candidates with complex metabolism-transporter interplay, are required to establish wider application of the ESF_{sd} method and confirm distinct trends between the preclinical species noted here. When using designated lots of human hepatocytes for assessment of new molecular entities, it would be prudent to evaluate uptake of a range of OATP substrates (low-medium-high clearance, different % active : passive contribution) to assess the need for ESF application from preclinical species.

In conclusion, the present study represents the most comprehensive assessment of OATP-mediated hepatic clearance performed to date in beagle dogs. In vitro uptake parameters obtained in this preclinical species showed low inter-individual variability with the exception of fexofenadine and pravastatin. Consistency in the extent of hepatocellular binding in three preclinical species and humans is encouraging and suggests that detailed mechanistic studies in preclinical species may be valuable to inform modelling of human hepatocyte data and subsequent PBPK model development. IVIVE of dog hepatocyte data resulted in a good agreement with the observed $CL_{int,H}$ (2.73-fold bias). The use of this value as an average empirical scaling factor improved human clearance IVIVE, suggesting utility of beagle dog as a preclinical model for the assessment of hepatic uptake mediated by OATPs. Use of dog ESF_{av} resulted in comparable success to monkey in improving human IVIVE, in contrast to use of drug specific scaling factors, rationalized by species differences in protein abundance and/or relative contribution of particular transporters mediating hepatic uptake. Further investigations and expansion of dataset to include cationic drugs and assessment of DDIs associated with transporter-mediated uptake (in isolation or in conjunction with metabolism and biliary excretion) would be informative to strengthen the use of dog as preclinical model for evaluation of transporter-mediated hepatic disposition.

Downloaded from dmd.aspetjournals.org at ASPET Journals on April 17, 2024

DMD Fast Forward. Published on December 28, 2018 as DOI: 10.1124/dmd.118.084194
This article has not been copyedited and formatted. The final version may differ from this version.

Acknowledgement

Authors would like to thank Dr David Hallifax and Ms Susan Murby for developing the methods of LC-MS/MS for in vitro hepatocytes experiments.

Downloaded from dmd.aspetjournals.org at ASPET Journals on April 17, 2024

DMD Fast Forward. Published on December 28, 2018 as DOI: 10.1124/dmd.118.084194
This article has not been copyedited and formatted. The final version may differ from this version.

Authorship contributions

Participated in research design: Norikazu Matsunaga, Bridget L. Morse, Kathleen M. Hillgren, Stephen D. Hall, J. Brian Houston, and Aleksandra Galetin

Conducted experiments: Norikazu Matsunaga, Bridget L. Morse, Michael A. Mohutsky, David W. Bedwell, and Jingqi Bao

Performed data analysis: Norikazu Matsunaga, Ayşe Ufuk, Bridget L. Morse

Wrote or contributed to the writing of the manuscript: Norikazu Matsunaga, Ayşe Ufuk, Bridget L. Morse, David W. Bedwell, Jingqi Bao, Michael A. Mohutsky, Kathleen M. Hillgren, Stephen D. Hall, J. Brian Houston, and Aleksandra Galetin

Downloaded from dmd.aspetjournals.org at ASPET Journals on April 17, 2024

DMD Fast Forward. Published on December 28, 2018 as DOI: 10.1124/dmd.118.084194
This article has not been copyedited and formatted. The final version may differ from this version.

References:

Barnett S, Ogungbenro K, Menochet K, Shen H, Lai Y, Humphreys WG, and Galetin A (2018) Gaining Mechanistic Insight Into Coproporphyrin I as Endogenous Biomarker for OATP1B-Mediated Drug-Drug Interactions Using Population Pharmacokinetic Modeling and Simulation. *Clin Pharmacol Ther* **104:**564-574.

Bow DA, Perry JL, Miller DS, Pritchard JB, and Brouwer KL (2008) Localization of P-gp (Abcb1) and Mrp2 (Abcc2) in freshly isolated rat hepatocytes. *Drug Metab Dispos* **36:**198-202.

Cantrill C and Houston JB (2017) Understanding the Interplay Between Uptake and Efflux Transporters Within In Vitro Systems in Defining Hepatocellular Drug Concentrations. *J Pharm Sci* **106:**2815-2825.

Chu X, Korzekwa KR, Elsby R, Fenner KS, Galetin A, Lai Y, Matsson P, Moss A, Nagar S, Rosania GR, Bai JPF, Polli JW, Sugiyama Y, and Brouwer KLR (2013) Intracellular Drug Concentrations and Transporters: Measurement, Modeling and Implications in the Liver. *Clin Pharmacol Ther* **94 (1)** :126-141.

Chu X, Shih SJ, Shaw R, Hentze H, Chan GH, Owens K, Wang S, Cai X, Newton D, Castro-Perez J, Salituro G, Palamanda J, Fernandis A, Ng CK, Liaw A, Savage MJ, and Evers R (2015) Evaluation of cynomolgus monkeys for the identification of endogenous biomarkers for hepatic transporter inhibition and as a translatable model to predict pharmacokinetic interactions with statins in humans. *Drug Metab Dispos* **43:**851-863.

De Bruyn T, Ufuk A, Cantrill C, Kosa RE, Bi YA, Niosi M, Modi S, Rodrigues AD, Tremaine LM, Varma MVS, Galetin A, and Houston JB (2018) Predicting Human Clearance of Organic Anion Transporting Polypeptide Substrates Using Cynomolgus Monkey: In Vitro-In Vivo Scaling of Hepatic Uptake Clearance. *Drug Metab Dispos* **46:**989-1000.

Deguchi T, Watanabe N, Kurihara A, Igeta K, Ikenaga H, Fusegawa K, Suzuki N, Murata S, Hirouchi M, Furuta Y, Iwasaki M, Okazaki O, and Izumi T (2011) Human pharmacokinetic prediction of UDP-glucuronosyltransferase substrates with an animal scale-up approach. *Drug Metab Dispos* **39:**820-829.

Galetin A, Zhao P, and Huang SM (2017) Physiologically Based Pharmacokinetic Modeling of Drug Transporters to Facilitate Individualized Dose Prediction. *J Pharm Sci* **106:**2204-2208.

Gertz M, Cartwright CM, Hobbs MJ, Kenworthy KE, Rowland M, Houston JB, and Galetin A (2013) Cyclosporine inhibition of hepatic and intestinal CYP3A4, uptake and efflux transporters: application of PBPK modeling in the assessment of drug-drug interaction potential. *Pharm Res* **30:**761-780.

Gertz M, Harrison A, Houston JB, and Galetin A (2010) Prediction of human intestinal first-pass metabolism of 25 CYP3A substrates from in vitro clearance and permeability data. *Drug Metab Dispos* **38:**1147-1158.

Downloaded from dmd.aspetjournals.org at ASPET Journals on April 17, 2024

DMD Fast Forward. Published on December 28, 2018 as DOI: 10.1124/dmd.118.084194
This article has not been copyedited and formatted. The final version may differ from this version.

Gill KL, Houston JB, and Galetin A (2012) Characterization of in vitro glucuronidation clearance of a range of drugs in human kidney microsomes: comparison with liver and intestinal glucuronidation and impact of albumin. *Drug Metab Dispos* **40:**825-835.

Gui C and Hagenbuch B (2010) Cloning/characterization of the canine organic anion transporting polypeptide 1b4 (Oatp1b4) and classification of the canine OATP/SLCO members. *Comparative biochemistry and physiology Toxicology & pharmacology : CBP* **151:**393-399.

Guo Y, Chu X, Parrott NJ, Brouwer KLR, Hsu V, Nagar S, Matsson P, Sharma P, Snoeys J, Sugiyama Y, Tatosian D, Unadkat JD, Huang SM, Galetin A, and International Transporter C (2018) Advancing Predictions of Tissue and Intracellular Drug Concentrations Using In Vitro, Imaging and Physiologically Based Pharmacokinetic Modeling Approaches. *Clin Pharmacol Ther* **104:**865-889.

Heikkinen AT, Friedlein A, Matondo M, Hatley OJ, Petsalo A, Juvonen R, Galetin A, Rostami-Hodjegan A, Aebersold R, Lamerz J, Dunkley T, Cutler P, and Parrott N (2015) Quantitative ADME proteomics - CYP and UGT enzymes in the Beagle dog liver and intestine. *Pharm Res* **32:**74-90.

Huang L, Berry L, Ganga S, Janosky B, Chen A, Roberts J, Colletti AE, and Lin MH (2010) Relationship between passive permeability, efflux, and predictability of clearance from in vitro metabolic intrinsic clearance. *Drug Metab Dispos* **38:**223-231.

Ito K and Houston JB (2005) Prediction of human drug clearance from in vitro and preclinical data using physiologically based and empirical approaches. *Pharm Res* **22:**103-112.

Izumi S, Nozaki Y, Maeda K, Komori T, Takenaka O, Kusuhara H, and Sugiyama Y (2015) Investigation of the impact of substrate selection on in vitro organic anion transporting polypeptide 1B1 inhibition profiles for the prediction of drug-drug interactions. *Drug Metab Dispos* **43:**235-247.

Jones HM, Barton HA, Lai Y, Bi YA, Kimoto E, Kempshall S, Tate SC, El-Kattan A, Houston JB, Galetin A, and Fenner KS (2012) Mechanistic pharmacokinetic modeling for the prediction of transporter-mediated disposition in humans from sandwich culture human hepatocyte data. *Drug Metab Dispos* **40:**1007-1017.

Jones HM, Chen Y, Gibson C, Heimbach T, Parrott N, Peters SA, Snoeys J, Upreti VV, Zheng M, and Hall SD (2015) Physiologically based pharmacokinetic modeling in drug discovery and development: a pharmaceutical industry perspective. *Clin Pharmacol Ther* **97**:247-262.

Li R, Bi YA, Lai Y, Sugano K, Steyn SJ, Trapa PE, and Di L (2014) Permeability comparison between hepatocyte and low efflux MDCKII cell monolayer. *The AAPS journal* **16:**802-809.

Mahmood I (1998) Interspecies scaling of renally secreted drugs. *Life sciences* **63:**2365-2371.

Ménochet K, Kenworthy KE, Houston JB, and Galetin A (2012a) Simultaneous assessment of uptake and metabolism in rat hepatocytes: a comprehensive mechanistic model. *J Pharmacol Exp Ther* **341:**2-15.

Downloaded from dmd.aspetjournals.org at ASPET Journals on April 17, 2024

DMD Fast Forward. Published on December 28, 2018 as DOI: 10.1124/dmd.118.084194
This article has not been copyedited and formatted. The final version may differ from this version.

Ménochet K, Kenworthy KE, Houston JB, and Galetin A (2012b) Use of Mechanistic Modelling to Assess Inter-Individual Variability and Inter-species Differences in Active Uptake in Human and Rat Hepatocytes. *Drug Metab Dispos* **40:**1744-1756.

Morse BL, Cai H, MacGuire JG, Fox M, Zhang L, Zhang Y, Gu X, Shen H, Dierks EA, Su H, Luk CE, Marathe P, Shu YZ, Humphreys WG, and Lai Y (2015) Rosuvastatin Liver Partitioning in Cynomolgus Monkeys: Measurement In Vivo and Prediction Using In Vitro Monkey Hepatocyte Uptake. *Drug Metab Dispos* **43**:1788-1794.

Naritomi Y, Terashita S, Kimura S, Suzuki A, Kagayama A, and Sugiyama Y (2001) Prediction of human hepatic clearance from in vivo animal experiments and in vitro metabolic studies with liver microsomes from animals and humans. *Drug Metab Dispos* **29:**1316-1324.

Noe J, Portmann R, Brun ME, and Funk C (2007) Substrate-dependent drug-drug interactions between gemfibrozil, fluvastatin and other organic anion-transporting peptide (OATP) substrates on OATP1B1, OATP2B1, and OATP1B3. *Drug Metab Dispos* **35:**1308-1314.

Prueksaritanont T, Subramanian R, Fang X, Ma B, Qiu Y, Lin JH, Pearson PG, and Baillie TA (2002) Glucuronidation of statins in animals and humans: a novel mechanism of statin lactonization. *Drug Metab Dispos* **30**:505-512.

Reinoso RF, Telfer BA, Brennan BS, and Rowland M (2001) Uptake of teicoplanin by isolated rat hepatocytes: comparison with in vivo hepatic distribution. *Drug Metab Dispos* **29**:453-459.

Riccardi K, Ryu S, Lin J, Yates P, Tess D, Li R, Singh D, Holder BR, Kapinos B, Chang G, and Di L (2018) Comparison of Species and Cell-Type Differences in Fraction Unbound of Liver Tissues, Hepatocytes, and Cell Lines. *Drug Metab Dispos* **46:**415-421.

Sall C, Houston JB, and Galetin A (2012) A comprehensive assessment of repaglinide metabolic pathways: impact of choice of in vitro system and relative enzyme contribution to in vitro clearance. *Drug Metab Dispos* **40:**1279-1289.

Shen H, Yang Z, Mintier G, Han YH, Chen C, Balimane P, Jemal M, Zhao W, Zhang R, Kallipatti S, Selvam S, Sukrutharaj S, Krishnamurthy P, Marathe P, and Rodrigues AD (2013) Cynomolgus monkey as a potential model to assess drug interactions involving hepatic organic anion transporting polypeptides: in vitro, in vivo, and in vitro-to-in vivo extrapolation. *J Pharmacol Exp Ther* **344:**673-685.

Shitara Y, Maeda K, Ikejiri K, Yoshida K, Horie T, and Sugiyama Y (2013) Clinical significance of organic anion transporting polypeptides (OATPs) in drug disposition: their roles in hepatic clearance and intestinal absorption. *Biopharm Drug Dispos* **34:**45-78.

Ufuk A, Kosa RE, Gao H, Bi YA, Modi S, Gates D, Rodrigues AD, Tremaine LM, Varma MVS, Houston JB, and Galetin A (2018) In Vitro-In Vivo Extrapolation of OATP1B-Mediated Drug-Drug Interactions in Cynomolgus Monkey. *J Pharmacol Exp Ther* **365:**688-699.

Downloaded from dmd.aspetjournals.org at ASPET Journals on April 17, 2024

DMD Fast Forward. Published on December 28, 2018 as DOI: 10.1124/dmd.118.084194
This article has not been copyedited and formatted. The final version may differ from this version.

Varma MV, Steyn SJ, Allerton C, and El-Kattan AF (2015) Predicting Clearance Mechanism in Drug Discovery: Extended Clearance Classification System (ECCS). *Pharm Res* **32:**3785-3802.

Wang L, Prasad B, Salphati L, Chu X, Gupta A, Hop CE, Evers R, and Unadkat JD (2015) Interspecies variability in expression of hepatobiliary transporters across human, dog, monkey, and rat as determined by quantitative proteomics. *Drug metabolism and disposition: the biological fate of chemicals* **43:**367-374.

Watanabe M, Watanabe T, Yabuki M, and Tamai I (2015) Dehydroepiandrosterone sulfate, a useful endogenous probe for evaluation of drug-drug interaction on hepatic organic anion transporting polypeptide (OATP) in cynomolgus monkeys. *Drug Metab Pharmacokinet* **30:**198-204.

Watanabe T, Kusuhara H, Watanabe T, Debori Y, Maeda K, Kondo T, Nakayama H, Horita S, Ogilvie BW, Parkinson A, Hu Z, and Sugiyama Y (2011) Prediction of the overall renal tubular secretion and hepatic clearance of anionic drugs and a renal drug-drug interaction involving organic anion transporter 3 in humans by in vitro uptake experiments. *Drug Metab Dispos* **39:**1031-1038.

Wilby AJ, Maeda K, Courtney PF, Debori Y, Webborn PJ, Kitamura Y, Kusuhara H, Riley RJ, and Sugiyama Y (2011) Hepatic uptake in the dog: comparison of uptake in hepatocytes and human embryonic kidney cells expressing dog organic anion-transporting polypeptide 1B4. *Drug Metab Dispos* **39:**2361-2369.

Wood FL, Houston JB, and Hallifax D (2017) Clearance Prediction Methodology Needs Fundamental Improvement: Trends Common to Rat and Human Hepatocytes/Microsomes and Implications for Experimental Methodology. *Drug Metab Dispos* **45:**1178-1188.

Yabe Y, Galetin A, and Houston JB (2011) Kinetic characterization of rat hepatic uptake of 16 actively transported drugs. *Drug Metab Dispos* **39:**1808-1814.

Yoshida K, Zhao P, Zhang L, Abernethy DR, Rekic D, Reynolds KS, Galetin A, and Huang SM (2017) In Vitro-In Vivo Extrapolation of Metabolism- and Transporter-Mediated Drug-Drug Interactions-Overview of Basic Prediction Methods. *J Pharm Sci*.

Yoshikado T, Toshimoto K, Nakada T, Ikejiri K, Kusuhara H, Maeda K, and Sugiyama Y (2017) Comparison of Methods for Estimating Unbound Intracellular-to-Medium Concentration Ratios in Rat and Human Hepatocytes Using Statins. *Drug Metab Dispos* **45:**779-789.

Zamek-Gliszczynski MJ, Lee CA, Poirier A, Bentz J, Chu X, Ishikawa T, Jamei M, Kalvass JC, Nagar S, Pang KS, Korzekwa K, Swaan PW, Taub ME, Zhao P, and Galetin A (2013) ITC Recommendations on Transporter Kinetic Parameter Estimation and Translational Modeling of Transport-Mediated PK and DDIs in Humans. *Clin Pharmacol Ther* **94 (1) :**64-79.

Downloaded from dmd.aspetjournals.org at ASPET Journals on April 17, 2024

DMD Fast Forward. Published on December 28, 2018 as DOI: 10.1124/dmd.118.084194
This article has not been copyedited and formatted. The final version may differ from this version.

Footnote

This work was supported by a consortium of pharmaceutical companies (GlaxoSmithKline, Lilly and Pfizer) within the Centre for Applied Pharmacokinetic Research at the University of Manchester.

Downloaded from dmd.aspetjournals.org at ASPET Journals on April 17, 2024

DMD Fast Forward. Published on December 28, 2018 as DOI: 10.1124/dmd.118.084194
This article has not been copyedited and formatted. The final version may differ from this version.

Figure Legends

Figure 1: Comparison of uptake parameters between humans and dogs

CL_{uptake} (A), $CL_{passive}$ (B), and CL_{active} (C) in plated dog hepatocytes scaled to per g of liver were compared with those in plated human hepatocytes (Ménochet et al., 2012b; De Bruyn et al., 2018). Data represent mean ± SD of n=3 dog hepatocyte donors. In human hepatocytes, data represent mean ± SD of n=4 donors (details in Table S6 footnote). The solid and dashed lines represent the line of unity and 2-fold difference, respectively. 1, cerivastatin; 2 fexofenadine; 3 pitavastatin; 4, pravastatin; 5, repaglinide; 6, rosuvastatin; 7, telmisartan; 8, valsartan

Figure 2: Comparison of uptake parameters among species

CL_{uptake} (A and B), $CL_{passive}$ (C and D), and CL_{active} (E and F) in plated dog hepatocytes were compared with those in rats (A, C, and E) (Ménochet et al., 2012a) and cynomolgus monkeys (B, D, and F) (De Bruyn et al., 2018). The solid and dashed lines represent the line of unity and 2-fold difference, respectively. 1, cerivastatin; 2, fexofenadine; 3, pitavastatin; 4, pravastatin; 5, repaglinide; 6, rosuvastatin; 7, telmisartan; 8, valsartan

Figure 3: Correlation of predicted and observed $CL_{int,H}$ in dogs

Predicted $CL_{int,H}$ values were compared to in vivo $CL_{int,H}$ in dogs. Predicted and observed data represent mean ± SD of n=3. The solid and dashed lines represent the line of unity and 2-fold difference, respectively. 1, atorvastatin; 2, cerivastatin; 3, fexofenadine; 4, pitavastatin; 5, pravastatin; 6, repaglinide; 7, rosuvastatin; 8, telmisartan; 9, valsartan

Figure 4: Correlation of predicted and observed $CL_{int,H}$ in humans in the absence of an empirical scaling factor, and direct comparison of the performance of ESFs from rat, dog and monkey in improving human $CL_{int,H}$ prediction

Predicted $CL_{int,H}$ values were compared to observed human $CL_{int,H}$ (A), and to precision error expressed as the log of predicted/observed $CL_{int,H}$ ratio either in the absence (B), or presence of drugset average (ESF_{av}) (C) and individual drug specific (ESF_{sd}) (D) empirical scaling factors. Human hepatocyte data

Downloaded from dmd.aspetjournals.org at ASPET Journals on April 17, 2024

DMD Fast Forward. Published on December 28, 2018 as DOI: 10.1124/dmd.118.084194
This article has not been copyedited and formatted. The final version may differ from this version.

represent mean ± SD of n=4 donors (details in Table S6 footnote). Error bars in panels C and D were excluded for clarity and distinction of preclinical species. The solid and dashed lines represent the line of unity and 2-fold difference, respectively. 1, cerivastatin; 2, fexofenadine; 3, pitavastatin; 4, pravastatin; 5, repaglinide; 6, rosuvastatin; 7, telmisartan; 8, valsartan; 9, bosentan

Figure 5: Correlation of predicted and observed $CL_{int,H}$ in humans using average and drug specific empirical scaling factors obtained from rat, dog and monkey

Predicted human $CL_{int,H}$ values were compared with in vivo human $CL_{int,H}$ following application of drugset average empirical scaling factors (ESF_{av}) (A, C and E), or individual drug specific empirical scaling factors (ESF_{sd}) (B, D and F) from dog (A-B), rat (C-D), and monkey (E-F). Predicted and observed $CL_{int,H}$ values in rats, monkey, and humans were previously reported (Supplemental Table S4, S5 and S6, respectively). Human hepatocyte data represent mean ± SD of n=4 donors (details in Table S6 footnote). The solid and dashed lines represent the line of unity and 2-fold difference, respectively. 1, cerivastatin; 2, fexofenadine; 3, pitavastatin; 4, pravastatin; 5, repaglinide; 6, rosuvastatin; 7, telmisartan; 8, valsartan; 9, bosentan

Figure 6: Residual plots for the prediction of in vivo intrinsic hepatic clearance $CL_{int,H}$ (mL/min/kg) in humans

Predicted $CL_{int,H}$ values were plotted against the precision error (log of predicted/observed $CL_{int,H}$ ratio) when using dataset average empirical scaling factors (ESF_{av}) (A, C, E), and individual drug specific empirical scaling factors (ESF_{sd}) (B, D, F) from dog (A, B), rat (C, D) and monkey (E, F). The solid and dashed lines represent the line of unity and 2-fold difference, respectively. 1, cerivastatin; 2, fexofenadine; 3, pitavastatin; 4, pravastatin; 5, repaglinide; 6, rosuvastatin; 7, telmisartan; 8, valsartan; 9, bosentan

Figure 7: Comparison of Kp parameters among species

Kp (A, B and C), Kp_{uu} (D, E and F), and fu_{cell} (G, H and I) in plated dog hepatocytes were compared with those in rats (A, D, and G) (Ménochet et al., 2012a), cynomolgus monkeys (B, E, and H) and humans (C, F and I) (De Bruyn et al., 2018). The solid and dashed lines represent the line of unity and 2-fold

Downloaded from dmd.aspetjournals.org at ASPET Journals on April 17, 2024

DMD Fast Forward. Published on December 28, 2018 as DOI: 10.1124/dmd.118.084194
This article has not been copyedited and formatted. The final version may differ from this version.

difference, respectively. 1, cerivastatin; 2, fexofenadine; 3, pitavastatin; 4, pravastatin; 5, repaglinide; 6, rosuvastatin; 7, telmisartan; 8, valsartan

Downloaded from dmd.aspetjournals.org at ASPET Journals on April 17, 2024

DMD Fast Forward. Published on December 28, 2018 as DOI: 10.1124/dmd.118.084194
This article has not been copyedited and formatted. The final version may differ from this version.

Table 1

Uptake parameters of 9 drugs investigated in dog hepatocytes

Drugs	CL_{uptake} (μL/min/10^6cells)	$CL_{passive}$ (μL/min/10^6cells)	CL_{active} (μL/min/10^6cells)	Active contribution (%)
Atorvastatin	107 ± 28	12.8 ± 1.5	94.6 ± 27.7	87.6 ± 2.7
Cerivastatin	143 ± 57	44.9 ± 23.7	98.5 ± 35.8	69.2 ± 6.1
Fexofenadine	9.44 ± 5.47	2.41 ± 2.24	7.03 ± 6.11	68.8 ± 23.4
Pitavastatin	112 ± 44	29.4 ± 7.4	82.5 ± 40.0	71.1 ± 11.2
Pravastatin	9.77 ± 3.24	1.28 ± 0.78	8.50 ± 3.36	86.2 ± 9.9
Repaglinide	135 ± 44	37.0 ± 10.0	98.1 ± 35.7	72.0 ± 5.8
Rosuvastatin	24.0 ± 1.7	1.91 ± 0.52	22.0 ± 2.1	91.9 ± 2.6
Telmisartan	135 ± 33	32.7 ± 9.1	102 ± 26	75.5 ± 4.2
Valsartan	30.3 ± 3.4	1.37 ± 0.65	28.9 ± 3.7	95.4 ± 2.6

Data represent mean ± S.D. from three lots of dog hepatocytes.

Downloaded from dmd.aspetjournals.org at ASPET Journals on April 17, 2024

DMD Fast Forward. Published on December 28, 2018 as DOI: 10.1124/dmd.118.084194
This article has not been copyedited and formatted. The final version may differ from this version.

Table 2

Kp parameters of 9 drugs investigated in dog hepatocytes

Drugs	Kp	$CL_{int,met}$ (μL/min/10^6cells)	Kp_{uu}	fu_{cell}
Atorvastatin	375 ± 117	1.94 ± 0.37	7.24 ± 1.54	0.021 ± 0.007
Cerivastatin	116 ± 19	–	3.34 ± 0.74	0.029 ± 0.007
Fexofenadine	38.5 ± 10.7	–	7.42 ± 8.80	0.168 ± 0.170
Pitavastatin	162 ± 25	–	3.81 ± 1.37	0.024 ± 0.011
Pravastatin	13.6 ± 2.4	–	9.54 ± 4.83	0.673 ± 0.267
Repaglinide	276 ± 78	24.8 ± 10.9	2.16 ± 0.47	0.008 ± 0.002
Rosuvastatin	26.4 ± 3.9	–	13.3 ± 4.1	0.509 ± 0.157
Telmisartan	308 ± 108	52.2 ± 21.6	1.62 ± 0.22	0.006 ± 0.001
Valsartan	307 ± 159	–	26.3 ± 13.3	0.097 ± 0.064

Data represent mean ± S.D. from three lots of dog hepatocytes. The $CL_{int,met}$ was determined from the slope of metabolite formation over time and was assumed to equal to the CL_{int} in eq. 2.

Downloaded from dmd.aspetjournals.org at ASPET Journals on April 17, 2024

DMD Fast Forward. Published on December 28, 2018 as DOI: 10.1124/dmd.118.084194
This article has not been copyedited and formatted. The final version may differ from this version.

Table 3

Pharmacokinetic parameters of 9 drugs investigated following intravenous administration in dogs

Drugs	CL_{total} (mL/min/kg)	CL_R (mL/min/kg)	CL_H (mL/min/kg)	fu_p	R_B
Atorvastatin	48.4 ± 13.3	ND	48.4 ± 13.3	0.057 ± 0.004	0.55[b]
Cerivastatin	2.48 ± 0.39	ND	2.48 ± 0.39	0.021 ± 0.001	0.76[c]
Fexofenadine	4.67 ± 1.42	0.401 ± 0.14	4.27 ± 1.30	0.134 ± 0.001	0.55[d]
Pitavastatin	5.86 ± 1.61	ND	5.86 ± 1.61	0.014 ± 0.002	0.60[e]
Pravastatin	14.1 ± 2.26	5.66[a]	10.4 ± 2.98	0.498 ± 0.02	0.60[e)]
Repaglinide	1.48 ± 0.47	ND	1.48 ± 0.47	0.003 ± 0.0001	0.48[c]
Rosuvastatin	23.2 ± 3.77	2.30 ± 1.23	20.9 ± 2.83	0.176 ± 0.006	0.56[c]
Telmisartan	17.4 ± 3.46	ND	17.4 ± 3.46	0.021 ± 0.003	1.18[f]
Valsartan	8.31 ± 1.33	0.475 ± 0.24	7.84 ± 1.45	0.010 ± 0.001	0.70[e]

Data represent mean ± S.D. from three male dogs intravenously infused. CL_H was determined by subtracting CL_R from CL_{total}.
ND, not determined (<1% total dose detected in urine)
[a]*no urine was collected in one of three animals, therefore CL_R is mean of 2 animals*
[b]*Gertz et al. (2010)*
[c]*Jones et al. (2012)*
[d]*Watanabe et al. (2011)*
[e]*Wilby et al. (2011)*
[f]*(Deguchi et al., 2011)*

Downloaded from dmd.aspetjournals.org at ASPET Journals on April 17, 2024

DMD Fast Forward. Published on December 28, 2018 as DOI: 10.1124/dmd.118.084194
This article has not been copyedited and formatted. The final version may differ from this version.

Table 4

Statistical data comparing the accuracy and precision of the use of species related empirical scaling factors (ESFs) to predict human $CL_{int,H.}$ Direct method involved no use of ESFs, and ESF_{av} and ESF_{sd} indicate the use of drugset average and individual drug specific ESFs, respectively.

		Species		
Methods	Parameters	Dog[b]	Rat	Monkey
N of drugs		8	9	9
Direct	gmfe	3.44	3.22	3.22
	rmse	3114	2936	2936
	% within 2-fold error	25	33	33
ESF_{av}[a]	gmfe	2.11	2.03	2.03
	rmse	2497	2392	2377
	% within 2-fold error	50	56	56
ESF_{sd}	gmfe	3.23	3.41	2.96
	rmse	2890	2957	3126
	% within 2-fold error	25	22	67

[a]The ESF_{av} values obtained in the IVIVE of preclinical CL_{uptake} data were 2.73, 2.61 and 2.66 in dog, rat and monkey, respectively; [b]Dataset excludes bosentan in dog (includes the remaining drugs: rosuvastatin, pitavastatin, cerivastatin, pravastatin, telmisartan, valsartan, repaglinide, fexofenadine)

Downloaded from dmd.aspetjournals.org at ASPET Journals on April 17, 2024

Figure 1

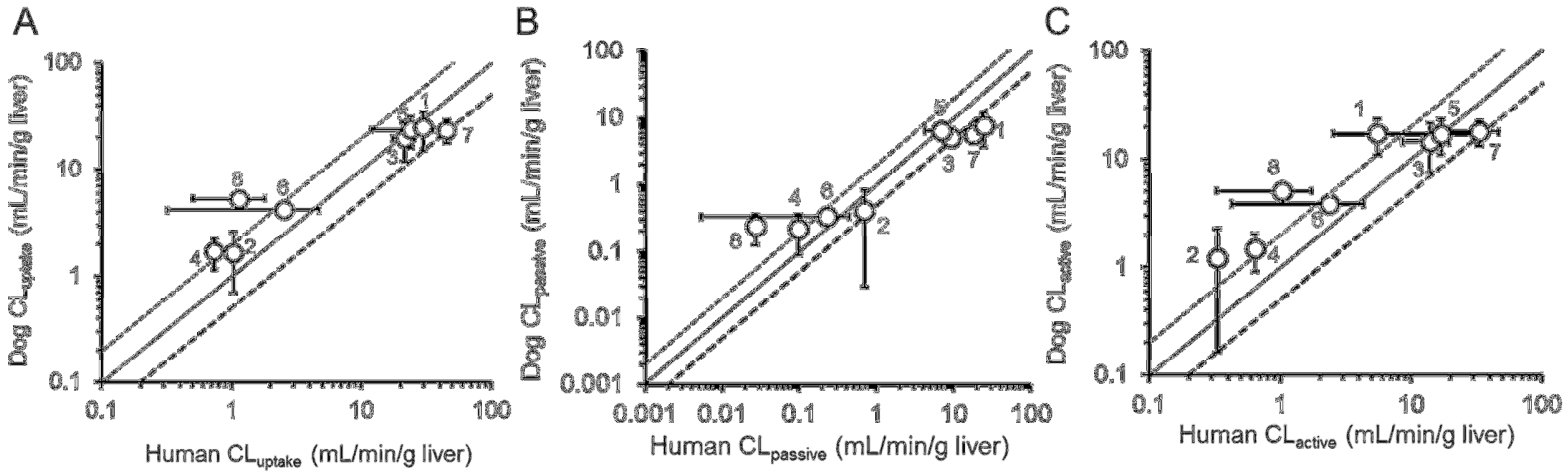

Downloaded from dmd.aspetjournals.org at ASPET Journals on April 17, 2024

DMD Fast Forward. Published on December 28, 2018 as DOI: 10.1124/dmd.118.084194
This article has not been copyedited and formatted. The final version may differ from this version.

DMD Fast Forward. Published on December 28, 2018 as DOI: 10.1124/dmd.118.084194
This article has not been copyedited and formatted. The final version may differ from this version.

Figure 2

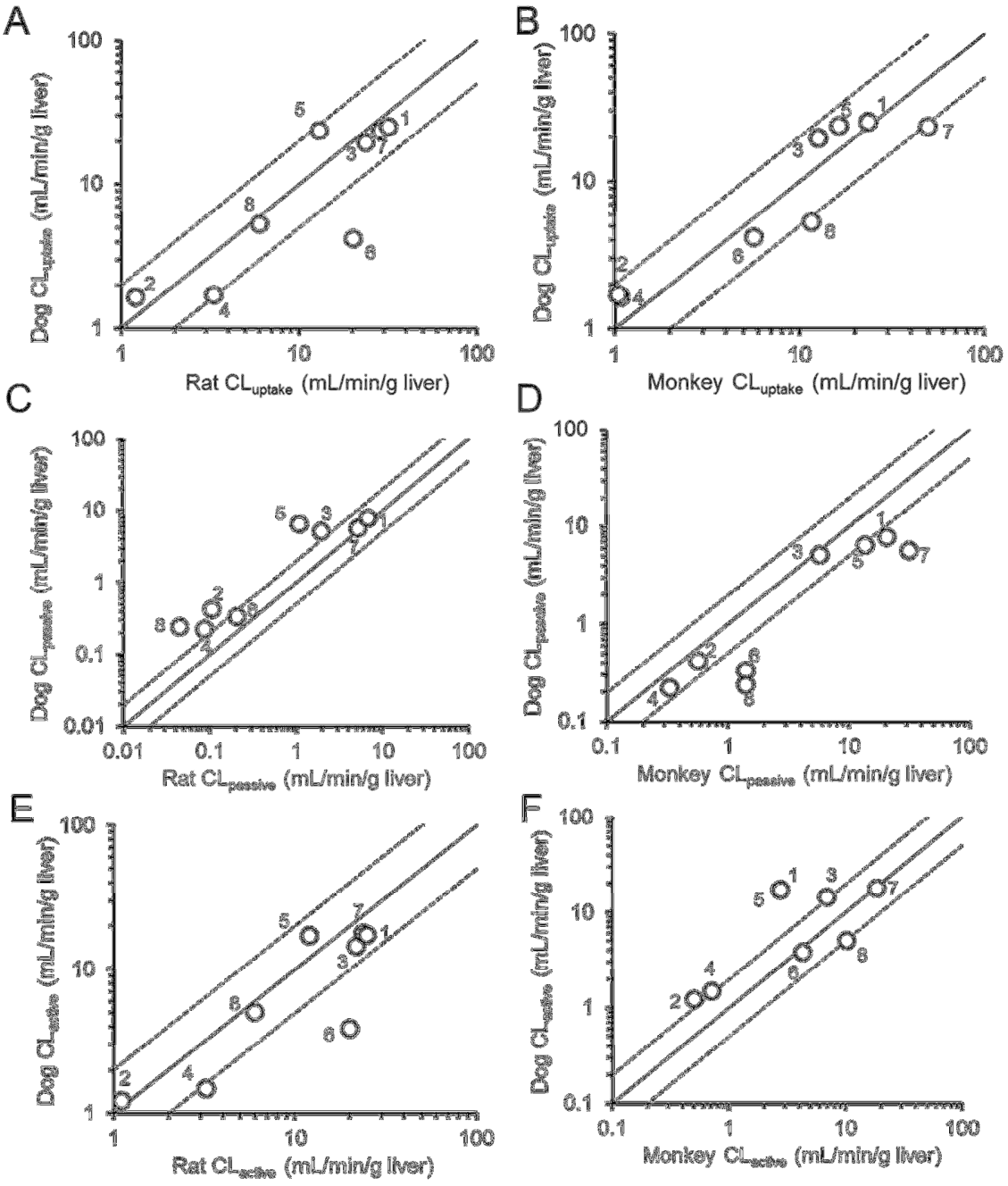

Downloaded from dmd.aspetjournals.org at ASPET Journals on April 17, 2024

DMD Fast Forward. Published on December 28, 2018 as DOI: 10.1124/dmd.118.084194
This article has not been copyedited and formatted. The final version may differ from this version.

Figure 3

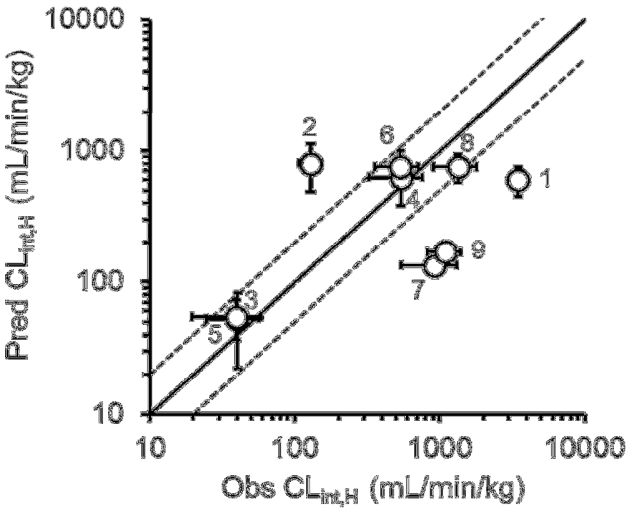

Downloaded from dmd.aspetjournals.org at ASPET Journals on April 17, 2024

DMD Fast Forward. Published on December 28, 2018 as DOI: 10.1124/dmd.118.084194
This article has not been copyedited and formatted. The final version may differ from this version.

Figure 4

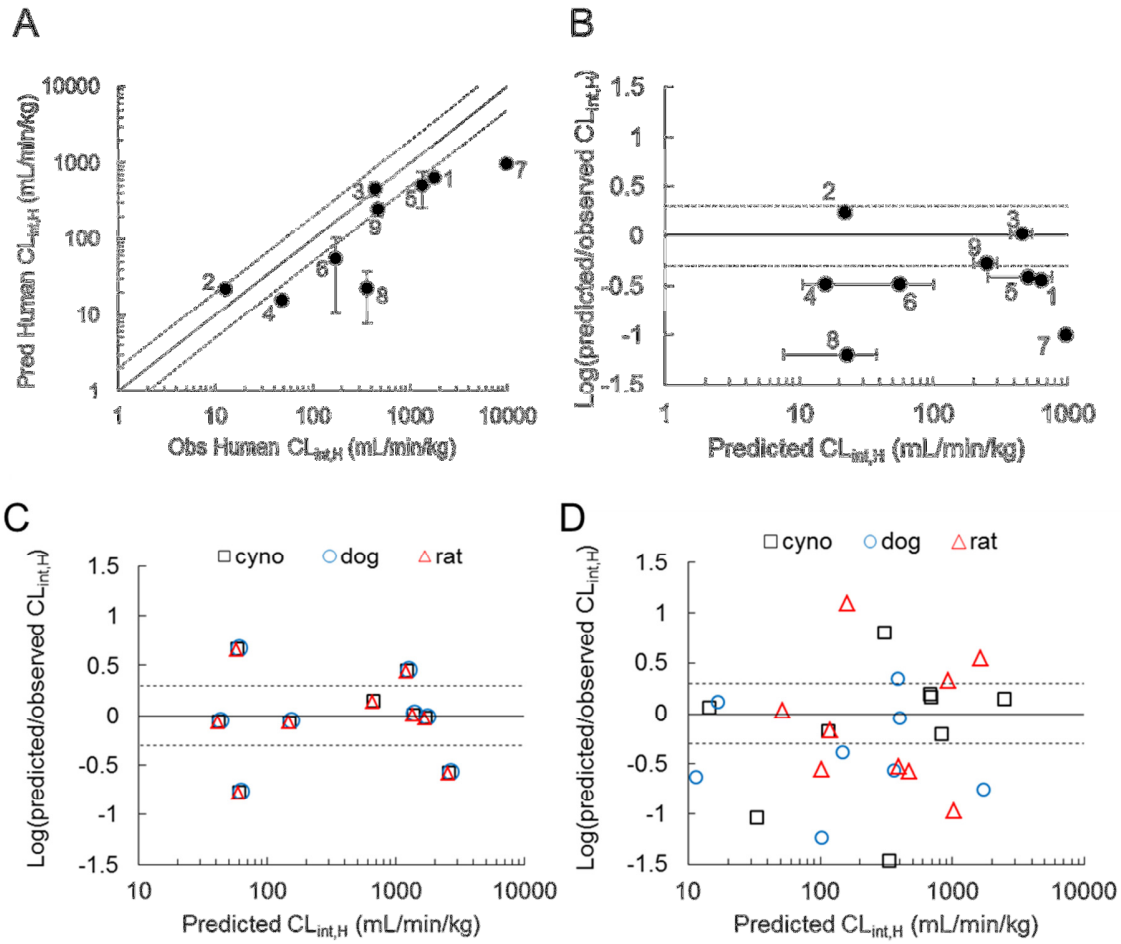

Downloaded from dmd.aspetjournals.org at ASPET Journals on April 17, 2024

DMD Fast Forward. Published on December 28, 2018 as DOI: 10.1124/dmd.118.084194
This article has not been copyedited and formatted. The final version may differ from this version.

Figure 5

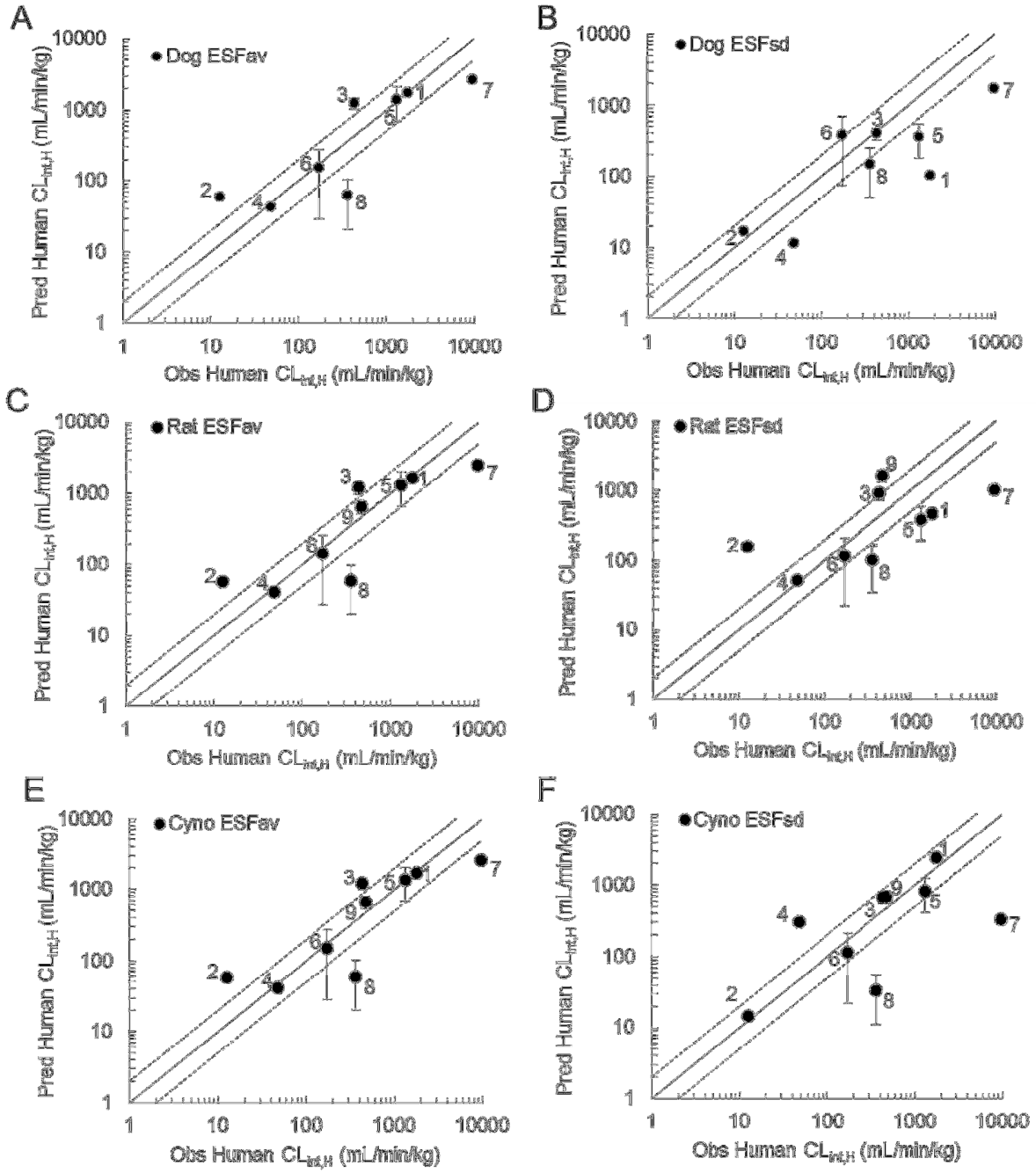

Downloaded from dmd.aspetjournals.org at ASPET Journals on April 17, 2024

DMD Fast Forward. Published on December 28, 2018 as DOI: 10.1124/dmd.118.084194
This article has not been copyedited and formatted. The final version may differ from this version.

Figure 6

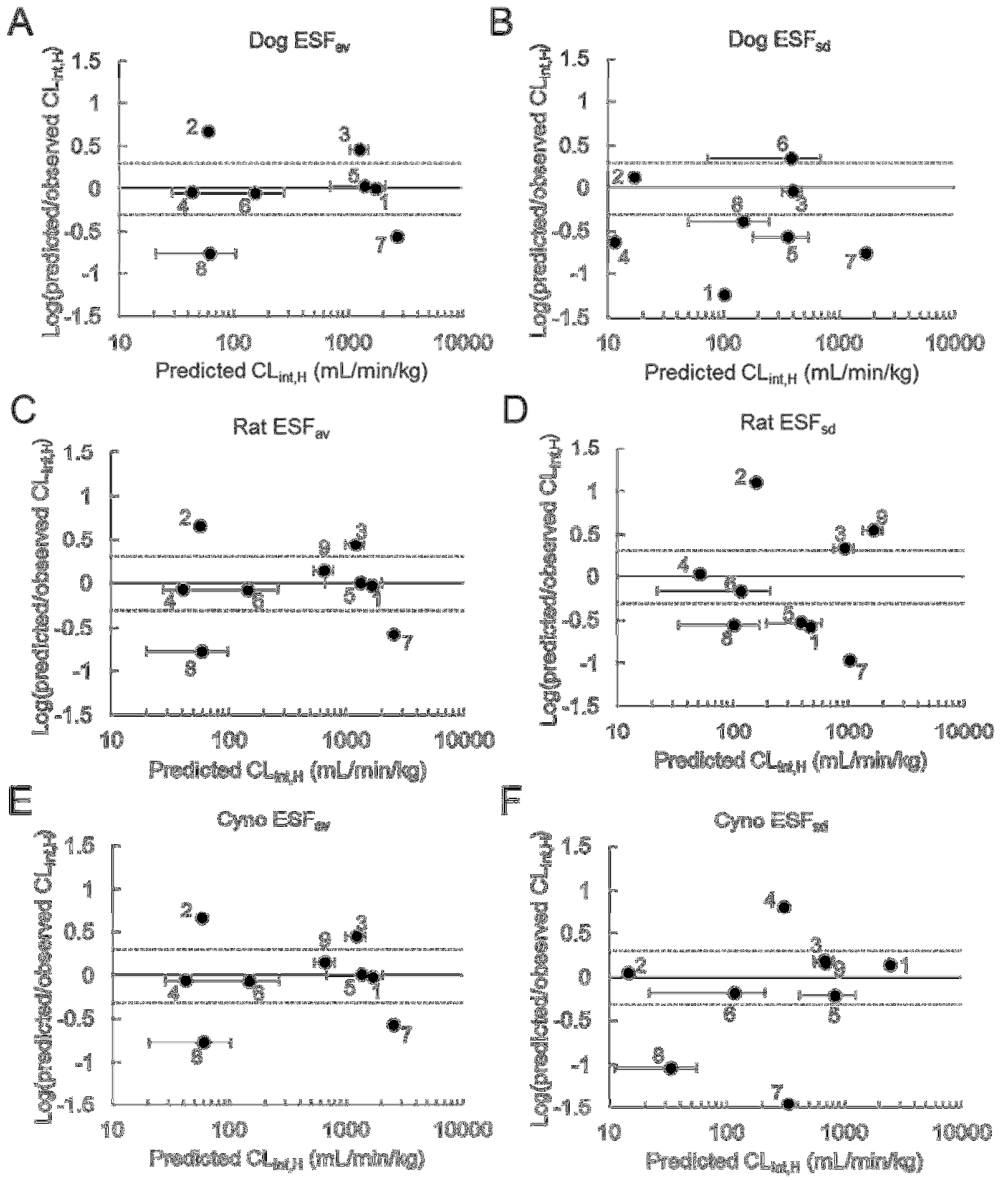

Downloaded from dmd.aspetjournals.org at ASPET Journals on April 17, 2024

DMD Fast Forward. Published on December 28, 2018 as DOI: 10.1124/dmd.118.084194
This article has not been copyedited and formatted. The final version may differ from this version.

Figure 7

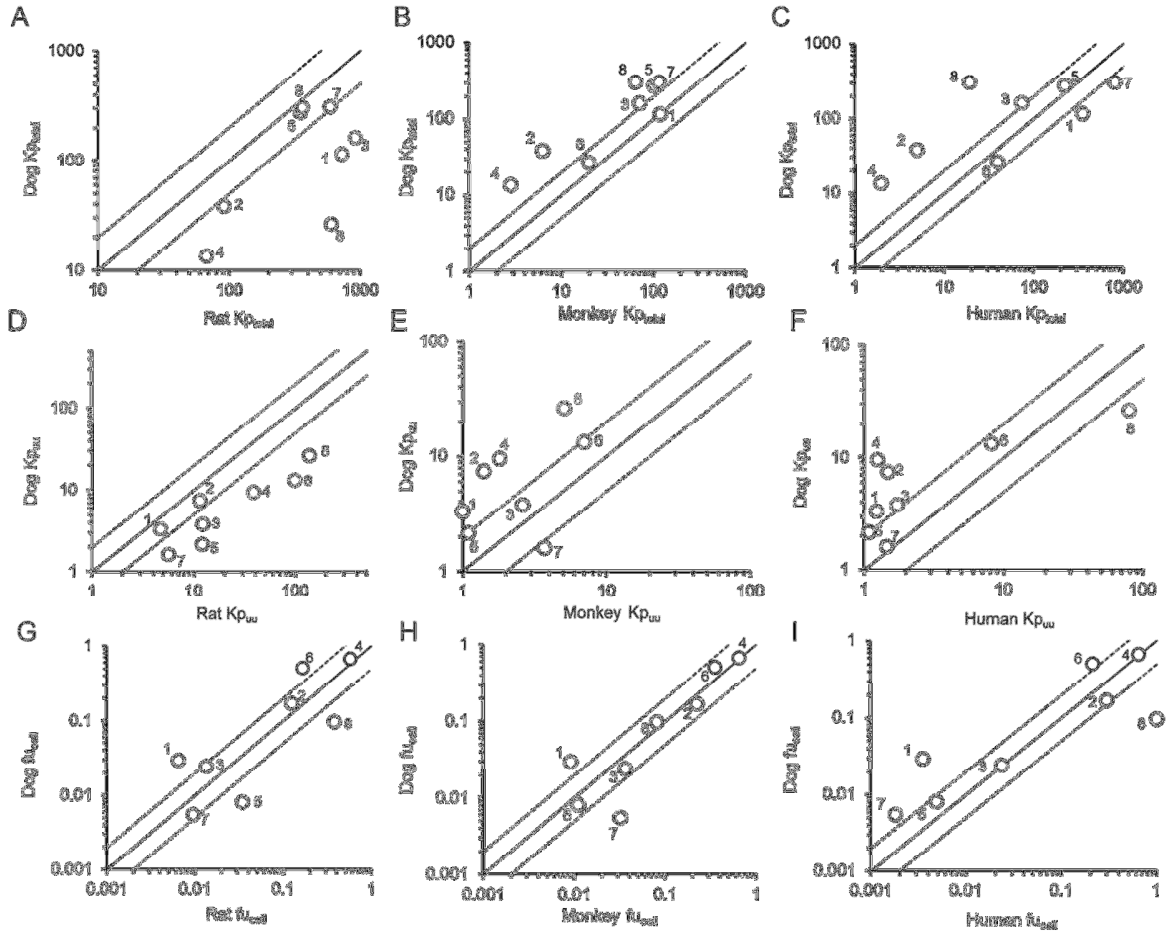

Downloaded from dmd.aspetjournals.org at ASPET Journals on April 17, 2024

Supplementary Material for the manuscript DMD#84194

Hepatic OATP-mediated clearance in the Beagle dog: assessing in vitro-in vivo relationships and applying cross species empirical scaling factors to improve prediction of human clearance

Norikazu Matsunaga, Ayşe Ufuk, Bridget L. Morse, David W. Bedwell, Jingqi Bao, Michael A. Mohutsky, Kathleen M. Hillgren, Stephen D. Hall, J. Brian Houston, and Aleksandra Galetin

Centre for Applied Pharmacokinetic Research, University of Manchester, UK (N.M., A.U., J.B.H., and A.G.), Pharmacokinetic Research Laboratories, Ono Pharmaceutical Co., Ltd., Japan (N.M.), and Lilly Research Laboratories, Eli Lilly and Company, USA (B.L.M., D.W.B., J.B., M.A.M., K.M.H., and S.D.H.)

Table S1: LC-MS/MS conditions for in vitro uptake and Kp experiments

Analyte (*m/z*)	Internal Standard (*m/z*)	Mobile Phase
Atorvastatin (559.3 → 440.4)	Diazepam (285.1 → 257.1)	A, B, D
Atorvastatin lactone (541.4 → 448.4)	Diazepam (285.1 → 257.1)	A, B, D
Cerivastatin (460.3 → 356.2)	Diazepam (285.1 → 257.1)	A, B, D
Fexofenadine (502.3 → 466.2)	Flunitrazepam (314.0 → 268.2)	C, D
Pitavastatin (422.3 → 290.3)	Atorvastatin (559.3 → 440.4)	A, B, C, D
Pravastatin (447.3 → 327.3)	Diazepam (285.1 → 257.1)	A, B, D
Repaglinide (453.3 → 230.2)	Diazepam (285.1 → 257.1)	A, B, D
Repaglinide glucuronide (629.4 → 230.4)	Diazepam (285.1 → 257.1)	A, B, D
Rosuvastatin (482.3 → 258.2)	Diazepam (285.1 → 257.1)	A, B, D
Telmisartan (515.1 → 276.1)	Diazepam (285.1 → 257.1)	A, B, D
Telmisartan glucuronide (691.5 → 515.4)	Diazepam (285.1 → 257.1)	A, B, D
Valsartan (436.5 → 235.5)	Diazepam (285.1 → 257.1)	A, B, D

A Waters Alliance 2795 connected with Waters Quattro Ultima triple quadruple mass spectrometer (Waters, Milford, MA) was used for LC MS/MS analyses. A Luna Phenyl Hexyl column 3 µm, 50 × 46 mm (Phenomenex, Torrance, CA) was used as an analytical column for drugs except for pitavastatin (Luna C18 column 3 µm, 50 × 46 mm).

A, 0.05% formic acid in water/methanol mixture (9:1, v/v); B, 0.05% formic acid in water/methanol (1:9, v/v); C, 1 mM ammonium acetate in water/methanol (9:1, v/v); D, 1 mM ammonium acetate in water/methanol (1:9, v/v)

Table S2: LC-MS/MS conditions for protein binding and in vivo studies

Analyte (*m/z*)	Internal Standard (*m/z*)	Mobile Phase
Atorvastatin (559.3 → 440.4)	Atorvastatin D5 (564.3 → 445.4)	A, B
Cerivastatin (461.3 → 356.3)	Eli Lilly Proprietary Compound	A, B
Fexofenadine (502.3 → 171.2)	Fexofenadine D6 (508.3 → 177.2)	A, C
Pitavastatin (422.3 → 290.3)	Eli Lilly Proprietary Compound	A, B
Pravastatin (423.2 → 321.0)	Pravastatin D3 (426.2 → 321.0)	A, B
Repaglinide (453.3 → 230.1)	Repaglinide D5 (458.3 → 230.1)	A, B
Rosuvastatin (482.2 → 258.2)	Rosuvastatin D6 (488.2 → 264.2)	C, D
Telmisartan (515.3 → 276.2)	Eli Lilly Proprietary Compound	A, E
Valsartan (436.2 → 207.1)	Valsartan D3 (439.2 → 208.1)	C, D

In vivo study samples were analyzed using a Sciex API 6500+ triple quadrupole mass spectrometer (Applied Biosystems/MDS; Foster City, CA) equipped with a TurboIonSpray interface. The pumps were Shimadzu LC-10AD units with a SCL-10A controller (Kyoto, Japan), and a CTC PAL liquid handler (Zwingen Switzerland) was used as the autosampler. Atorvastatin, fexofenadine, pravastatin, repaglinide, telmisartan and valsartan were analyzed using a Kinetex XB C18 2 x 30 column. Cerivastatin and pitavastatin wereanalyzed using an Ace UltraCore SuperC18 2.1 x 30 column and rosuvastatin analyzed using an Betasil javelin C18 2.1 x 20 column.

A, 2M ammonium bicarbonate/ water (25:1000 v/v); B, 2M ammonium bicarbonate/methanol (25:1000 v/v); C, acetonitrile; D, formic acid/ water (10:1000 v/v); E, methanol

Table S3: Data sources for physiological parameters in dogs

Parameters	References				Median
Hepatocellularity (10^6 cells/g liver)	240[a]	135[b]	215[c]	120[d]	175
Liver weight (g liver/kg)	29.1[e]	32.9[f]	32[g]	32[d]	32
Hepatic blood flow (mL/min/kg)	41.0[e]	41.5[f]	30.9[g]	33[d]	40

[a]Bayliss et al. (1999)
[b]Szákacs et al. (2001)
[c]Sohlenius-Sternbeck (2006)
[d]Peters (2012)
[e]Boxenbaum (1980)
[d]Brown et al. (1997)
[f]Davies and Morris (1993)

Table S4: In vivo and in vitro clearance data in rats

	In vivo CL_{total} (mL/min/kg)	In vivo CL_R (mL/min/kg)	In vivo CL_H (mL/min/kg)	fu_p	R_B	Observed $CL_{int,H}$ (mL/min/kg)	In vitro CL_{uptake} (µL/min/10^6cells)	Predicted $CL_{int,H}$ (mL/min/kg)	Fold error
Cerivastatin	17.00[a]	-	17.00	0.026[a]	0.70[a]	938.9	265[b]	1273	0.74
Fexofenadine	52.80[d]	8.20[d]	44.60	0.338[d]	0.895[d]	349.9	10.07[e]	48	7.24
Pitavastatin	18.20[f]	-	18.20[f]	0.014[f]	0.65[f]	2000.0	207[g]	994	2.01
Pravastatin	43.70[h)]	-	43.70[h]	0.672[h]	0.65[h]	407.4	26[g]	123	3.30
Repaglinide	5.28[i]	-	5.28[i]	0.015[j]	0.62[j]	393.9	107[g]	512	0.77
Rosuvastatin	28.00[h)]	0.032[k]	27.97	0.039[h]	0.60[h]	1718.4	169[g]	813	2.11
Telmisartan	6.75[l]	-	6.75	0.006[l]	1.00[l]	1228.7	240[g]	1154	1.06
Valsartan	4.20[h]	-	4.20	0.004[h]	0.66[h]	1140.7	53[g]	255	4.47
Bosentan	23.00[m]	-	23.00	0.011[n]	0.55[p]	4381.0	138[g]	661	6.63

CL_H was determined from CL_{total} and CL_R. Observed $CL_{int,H}$ was calculated by the well-stirred model shown in eq. 9 with rat hepatic blood flow 80 mL/min/kg[q]. The in vitro CL_{uptake} was scaled by a hepatocellularity value of 120 × 10^6 cells/g liver and rat liver weight of 40 g liver/body weight[q].

[a]Paine et al. (2008)

[b]In house data (265 ± 91 µL/min/10^6 cells, n=3 separate experiments) measured after 2 h culture, followed by uptake studies performed at 1 µM over 2 min as previously[c)]

[c]De Bruyn et al. (2018)

[d]Poirier et al. (2008)

[e]Estimated over 0.1-100 µM range using the conventional 2-step method as reported by Cantrill and Houston (2017)

[f]Watanabe et al. (2010)

[g]In vitro CL_{uptake} values were from Ménochet et al. (2012a): parameters were estimated over 0.1-300 µM range using the mechanistic 2-compartment model and corrected for the loss of cells during experiment

[h]Fukuda et al. (2008)

[i]Li and Jiang (2012)

[j]Xiao et al. (2015)
[k]Nezasa et al. (2002)
[l]Gardiner and Paine (2011)
[m]Treiber et al. (2004)
[n]Calculated from $R_B=fu_p/fu_b$ with $fu_b=0.02$[o]
[o]Lave et al. (1997)
[p]Haematocrit
[q]Peters (2012)

Table S5: Individual uptake parameters obtained in the three lots of plated dog hepatocytes

Drugs	Parameters	XVD	XZG	YHF
Atorvastatin	CL_{total} (μL/min/10^6cells)	140	90.7	91.5
	$CL_{passive}$ (μL/min/10^6cells)	13.5	11.1	13.9
	CL_{active} (μL/min/10^6cells)	127	79.5	77.7
Cerivastatin	CL_{total} (μL/min/10^6cells)	203	137	90.1
	$CL_{passive}$ (μL/min/10^6cells)	72.2	32.7	29.8
	CL_{active} (μL/min/10^6cells)	131	104	60.3
Fexofenadine	CL_{total} (μL/min/10^6cells)	14.8	9.62	3.88
	$CL_{passive}$ (μL/min/10^6cells)	0.843	4.98	1.40
	CL_{active} (μL/min/10^6cells)	14.0	4.65	2.47
Pitavastatin	CL_{total} (μL/min/10^6cells)	146	128	62.0
	$CL_{passive}$ (μL/min/10^6cells)	38.0	24.8	25.6
	CL_{active} (μL/min/10^6cells)	108	103	36.4
Pravastatin	CL_{total} (μL/min/10^6cells)	13.5	8.41	7.44
	$CL_{passive}$ (μL/min/10^6cells)	1.11	2.12	0.596
	CL_{active} (μL/min/10^6cells)	12.4	6.29	6.85
Repaglinide	CL_{total} (μL/min/10^6cells)	185	118	103
	$CL_{passive}$ (μL/min/10^6cells)	47.6	27.8	35.7
	CL_{active} (μL/min/10^6cells)	137	89.8	67.3
Rosuvastatin	CL_{total} (μL/min/10^6cells)	22.9	23.1	25.9
	$CL_{passive}$ (μL/min/10^6cells)	2.48	1.75	1.49
	CL_{active} (μL/min/10^6cells)	20.4	21.3	24.4
Telmisartan	CL_{total} (μL/min/10^6cells)	169	130	104
	$CL_{passive}$ (μL/min/10^6cells)	43.1	25.8	29.3
	CL_{active} (μL/min/10^6cells)	126	104	75.1
Valsartan	CL_{total} (μL/min/10^6cells)	27.3	29.7	34.0
	$CL_{passive}$ (μL/min/10^6cells)	2.04	0.742	1.33
	CL_{active} (μL/min/10^6cells)	25.2	28.9	32.6

Data represent the mean value in triplicate.

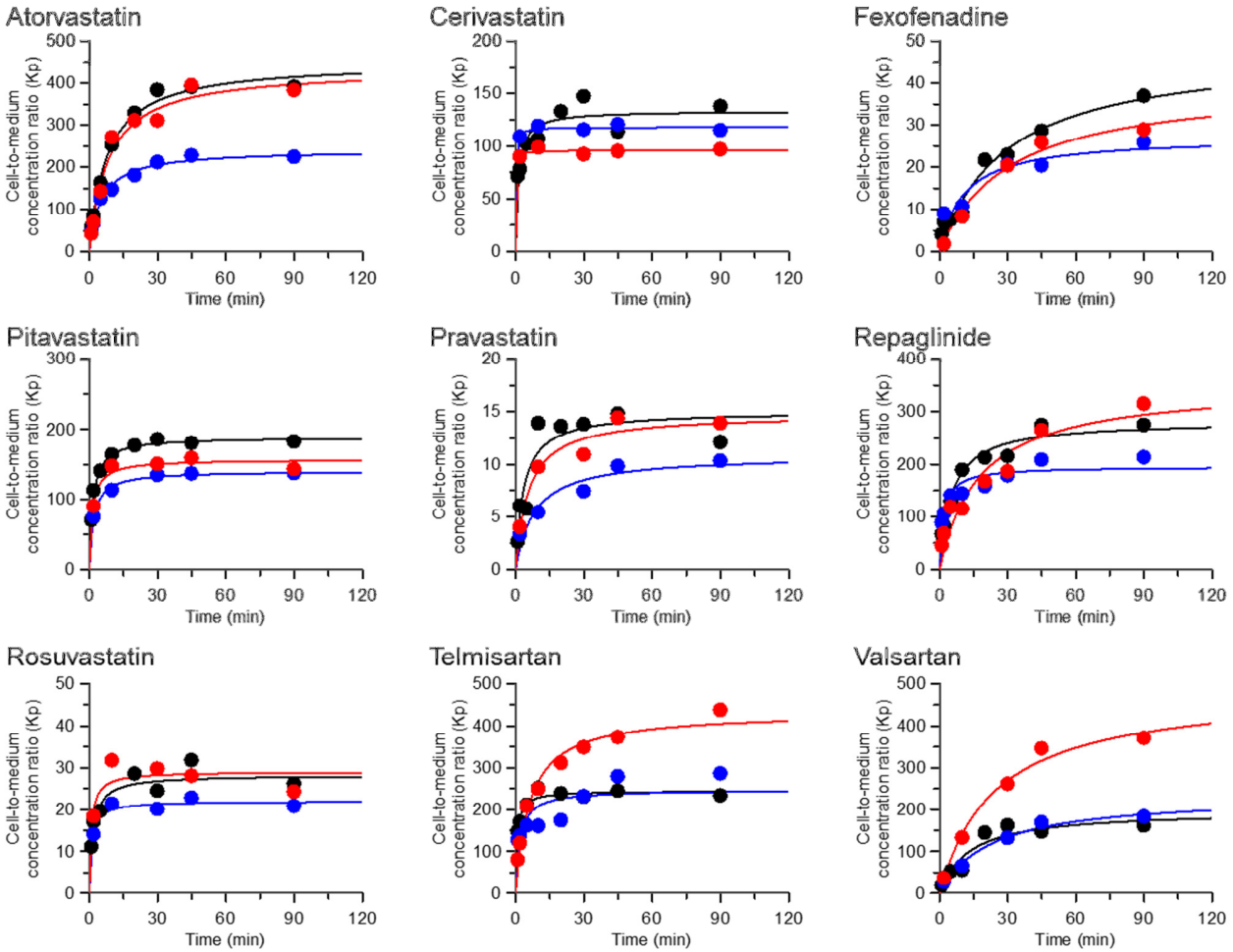

Figure S1: Cell-to-medium concentration ratio (Kp)-time profiles of 9 OATP substrates in three lots of plated dog hepatocytes

Black, blue and red symbols represent the observed data for donors XVD, XZG and YHF, respectively. The solid lines represent the fitting for the corresponding donors. A hyperbolic curve fitting was performed in GraFit v6.0.6 to estimate the maximum Kp at equilibrium.

Table S6: Individual Kp, Kp_{uu} and $f_{u,cell}$ parameters obtained in three lots of plated dog hepatocytes

Drugs	Parameters	XVD	XZG	YHF
Atorvastatin	Kp	450	240	434
	Kp_{uu}	8.95	6.81	5.96
	fu_{cell}	0.020	0.028	0.014
Cerivastatin	Kp	133	118	95.7
	Kp_{uu}	2.82	4.18	3.02
	fu_{cell}	0.021	0.035	0.032
Fexofenadine	Kp	48.2	27.1	40.2
	Kp_{uu}	17.6	1.93	2.76
	fu_{cell}	0.365	0.071	0.069
Pitavastatin	Kp	189	140	157
	Kp_{uu}	3.84	5.17	2.43
	fu_{cell}	0.020	0.037	0.015
Pravastatin	Kp	15.0	10.8	14.8
	Kp_{uu}	12.2	3.96	12.5
	fu_{cell}	0.809	0.365	0.845
Repaglinide	Kp	282	195	352
	Kp_{uu}	2.69	1.81	1.98
	fu_{cell}	0.010	0.009	0.006
Rosuvastatin	Kp	28.2	22.0	29.0
	Kp_{uu}	9.23	13.2	17.4
	fu_{cell}	0.327	0.600	0.599
Telmisartan	Kp	244	247	433
	Kp_{uu}	1.62	1.39	1.84
	fu_{cell}	0.007	0.006	0.004
Valsartan	Kp	197	234	489
	Kp_{uu}	13.4	40.0	25.5
	fu_{cell}	0.068	0.171	0.052

Data represent the mean value in duplicate.

Table S7: Comparison of estimated CL_{active}, $CL_{passive}$ and fu_{cell} of rosuvastatin from short and long incubation periods in plated dog hepatocytes (lot XVD)

Drugs	Parameters	Short incubation (from initial uptake rate and eq. 3)	Long incubation (by mechanistic modelling, eq. 4-5)
Cerivastatin	CL_{active} (µL/min/10^6cells)	131	201
	$CL_{passive}$ (µL/min/10^6cells)	72.2	136
	fu_{cell}	0.021	0.010
Fexofenadine	CL_{active} (µL/min/10^6cells)	14	6.93
	$CL_{passive}$ (µL/min/10^6cells)	0.843	0.545
	fu_{cell}	0.365	0.391
Pitavastatin	CL_{active} (µL/min/10^6cells)	108	149
	$CL_{passive}$ (µL/min/10^6cells)	38	70.8
	fu_{cell}	0.024	0.025
Pravastatin	CL_{active} (µL/min/10^6cells)	12.4	12.7
	$CL_{passive}$ (µL/min/10^6cells)	1.11	2.20
	fu_{cell}	0.809	0.611
Rosuvastatin	CL_{active} (µL/min/10^6cells)	20.4	15.3
	$CL_{passive}$ (µL/min/10^6cells)	2.48	1.51
	fu_{cell}	0.327	0.293
Valsartan	CL_{active} (µL/min/10^6cells)	25.2	34.2
	$CL_{passive}$ (µL/min/10^6cells)	2.04	2.73
	fu_{cell}	0.068	0.102

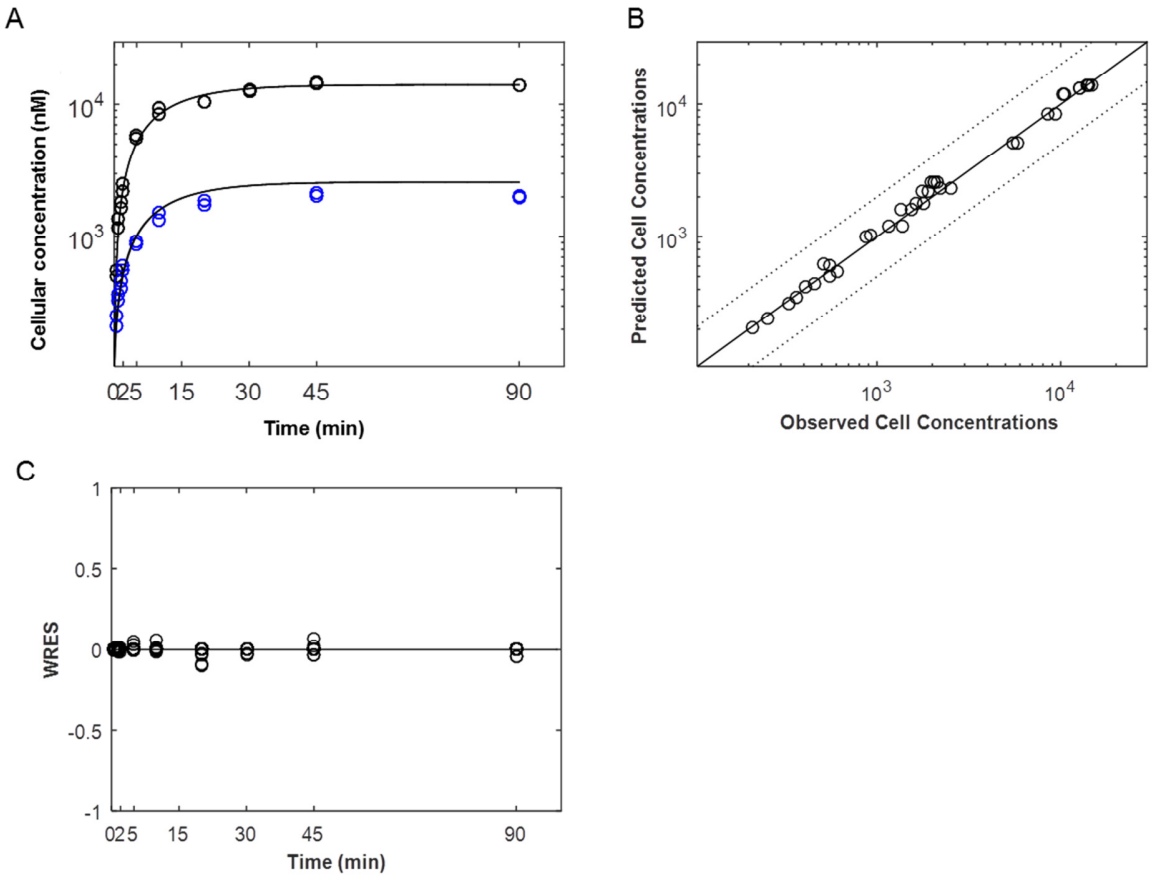

Figure S2: Two compartment mechanistic modelling of rosuvastatin concentration-time profile

Panel A shows cell concentration vs. time profile of rosuvastatin with symbols and black line representing the observed data and model fitting, respectively. Black and blue symbols represent the data in the absence and presence of the cocktail inhibitor. Panel B and C show the goodness of fit and weighted residual error vs. time plots, respectively. The solid and dotted lines in panels B and C represent the line of unity and the 2-fold error, respectively.

Table S8: In vivo and in vitro clearance data in cynomolgus monkeys

	In vivo CL_{total} (mL/min/kg)[a]	In vivo CL_R (mL/min/kg)[a]	In vivo CL_H (mL/min/kg)	fu_p[a]	R_B[a]	Observed $CL_{int,H}$ (mL/min/kg)	In vitro CL_{uptake} (µL/min/10^6cells)[a]	Predicted $CL_{int,H}$ (mL/min/kg)	Fold error
Cerivastatin	19.00	-	19.00	0.014	0.76	3181	223	817.0	3.89
Fexofenadine	6.54	1.67[a]	4.87	0.310	0.55	19	8.00	29.4	0.66
Pitavastatin	10.90	0.11[a]	10.80	0.026	0.58	723	134	491.7	1.47
Pravastatin	30.00	6.93[a]	23.10	0.650	0.56	644	9.00	33.0	19.48
Repaglinide	6.89	-	6.89	0.012	0.62	771	129	473.7	1.63
Rosuvastatin	23.70	4.27[a)]	19.40	0.180	0.69	305	40.1	147.2	2.07
Telmisartan	9.00	-	9.00	0.025	0.78	490	387	1420.7	0.34
Valsartan	6.53	0.62[a]	5.91	0.014	0.55	560	105	384.8	1.46
Bosentan	17.90	-	17.90	0.061	0.66	776	77.0	281.3	2.76

CL_H was determined from CL_{total} and CL_R. Observed $CL_{int,H}$ was calculated by the well-stirred model shown in eq. 9 with monkey hepatic blood flow 43.6 mL/min/kg[b]. The in vitro CL_{uptake} was scaled by a hepatocellularity value of 120×10^6 cells/g liver and monkey liver weight of 30 g liver/body weight[b]. R_B values were assumed to be the same as those in humans.

[a]De Bruyn et al. (2018)

[b]Davies and Morris (1993)

Table S9: In vivo and in vitro clearance data in humans

	In vivo CL_{total} (mL/min/kg)[a]	In vivo CL_R (mL/min/kg)[a]	In vivo CL_H (mL/min/kg)[a]	fu_p[a]	R_B[a]	Observed $CL_{int,H}$ (mL/min/kg)[a]	In vitro CL_{uptake} (µL/min/10^6cells)[b]	Predicted $CL_{int,H}$ (mL/min/kg)	Fold error
Cerivastatin	2.90	-	2.90	0.002	0.76	1778	244.0	639.1	2.78
Fexofenadine	3.10	1.2	1.9	0.18	0.55	13	8.4	22.0	0.58
Pitavastatin	5.7	-	5.7	0.025	0.58	434	175.6 ± 33.4	459.9 ± 87.6	0.94
Pravastatin	14	6.6	7.4	0.43	0.56	48	6.0	15.8	3.04
Repaglinide	7.8	-	7.8	0.015	0.62	1326	195.2 ± 98.1	511.4 ± 256.9	2.59
Rosuvastatin	10.5	2.9	7.6	0.094	0.69	172	21.3 ± 17.3	55.8 ± 45.3	3.08
Telmisartan	12	-	12	0.005	0.78	9657	370.3 ± 24.4	970.1 ± 63.8	9.96
Valsartan	0.49	0.14	0.35	0.001	0.55	361	8.7 ± 5.8	22.8 ± 15.2	15.8
Bosentan	2.10	-	2.10	0.0053	0.66	468	95.2 ± 18.7	249.3 ± 49.0	1.88

CL_H was determined from CL_{total} and CL_R. Observed $CL_{int,H}$ was calculated by the well-stirred model shown in eq. 9 with human hepatic blood flow 20.7 mL/min/kg[d]. The in vitro CL_{uptake} was scaled by a hepatocellularity value of 120×10^6 cells/g liver and human liver weight of 21.4 g liver/body weight[e].

[a]De Bruyn et al. (2018)

[b]Data represent mean ± SD of n=4 donors reported in De Bruyn et al. (2018) and Ménochet et al. (2012b)[c], except for pravastatin (n=2), cerivastatin (n=1) and fexofenadine (n=1). The same applies for CL_{active} whereas for $CL_{passive}$, represent mean of n=2 donors except for cerivastatin and fexofenadine (n=1), and rosuvastatin and repaglinide (n=4) (Ménochet et al., 2012b; De Bruyn et al., 2018)

[c]Data from Ménochet et al. (2012b) were corrected for cell loss during uptake experiment

[d]Davies and Morris (1993)

[e]Rawden et al. (2005)

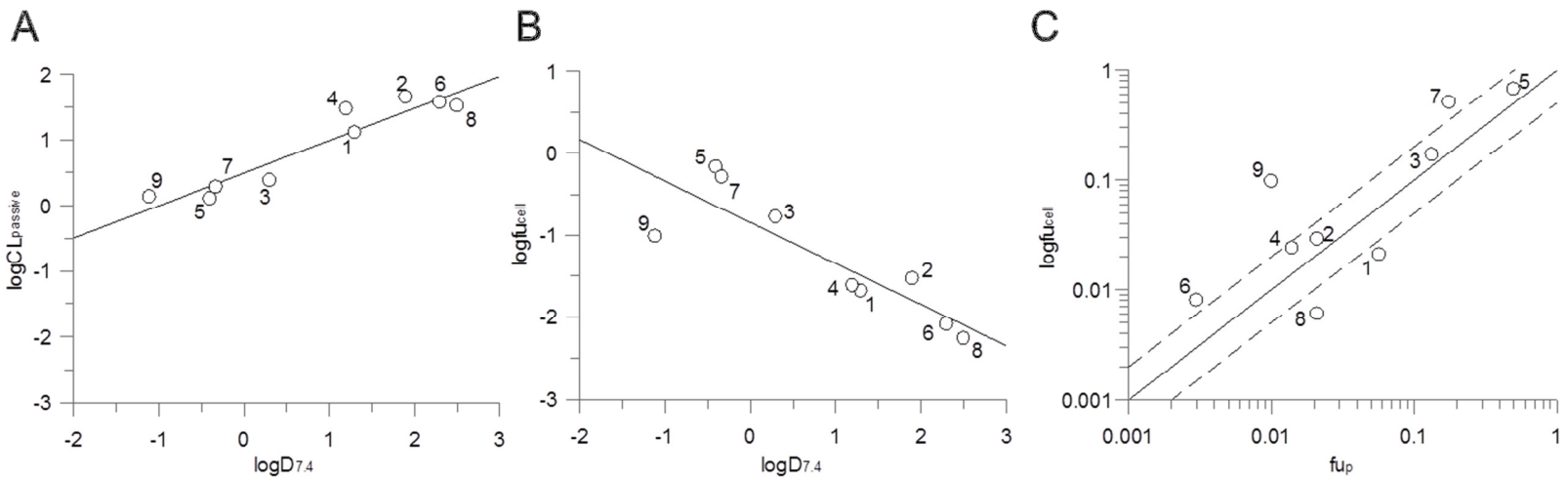

Figure S3: Correlation of $CL_{passive}$ and fu_{cell} values with physicochemical properties $logD_{7.4}$ and relationship between fu_{cell} and fu_p

The log-transformed $CL_{passive}$ (A) and fu_{cell} (B) values of 9 drugs investigated were compared with their physicochemical properties, $logD_{7.4}$. Correlation between the observed fu_{cell} and fu_p (C) of 9 drugs was investigated. (A) Relationship between parameters was described by the following equation: $logCL_{passive} = 0.492 \times logD_{7.4} + 0.494$ ($r^2 = 0.893$). (B) The solid and dashed lines represent the line of unity and 2-fold difference, respectively. (C) Relationship between parameters was described by the following equation: $logfu_{cell} = -0.502 \times logD_{7.4} - 0.843$ ($r^2 = 0.751$). 1, atorvastatin; 2, cerivastatin; 3, fexofenadine; 4, pitavastatin; 5, pravastatin; 6, repaglinide; 7, rosuvastatin; 8, telmisartan; 9, valsartan

References

Bayliss MK, Bell JA, Jenner WN, Park GR, and Wilson K (1999) Utility of hepatocytes to model species differences in the metabolism of loxtidine and to predict pharmacokinetic parameters in rat, dog and man. *Xenobiotica* **29:**253-268.

Boxenbaum H (1980) Interspecies variation in liver weight, hepatic blood flow, and antipyrine intrinsic clearance: extrapolation of data to benzodiazepines and phenytoin. *J Pharmacokinet Biopharm* **8:**165-176.

Brown RP, Delp MD, Lindstedt SL, Rhomberg LR, and Beliles RP (1997) Physiological parameter values for physiologically based pharmacokinetic models. *Toxicol Ind Health* **13:**407-484.

Cantrill C and Houston JB (2017) Understanding the Interplay Between Uptake and Efflux Transporters Within In Vitro Systems in Defining Hepatocellular Drug Concentrations. *J Pharm Sci* **106:**2815-2825.

Davies B and Morris T (1993) Physiological parameters in laboratory animals and humans. *Pharm Res* **10:**1093-1095.

De Bruyn T, Ufuk A, Cantrill C, Kosa RE, Bi YA, Niosi M, Modi S, Rodrigues AD, Tremaine LM, Varma MVS, Galetin A, and Houston JB (2018) Predicting Human Clearance of Organic Anion Transporting Polypeptide Substrates Using Cynomolgus Monkey: In Vitro-In Vivo Scaling of Hepatic Uptake Clearance. *Drug Metab Dispos* **46:**989-1000.

Fukuda H, Ohashi R, Tsuda-Tsukimoto M, and Tamai I (2008) Effect of plasma protein binding on in vitro-in vivo correlation of biliary excretion of drugs evaluated by sandwich-cultured rat hepatocytes. *Drug Metab Dispos* **36:**1275-1282.

Gardiner P and Paine SW (2011) The impact of hepatic uptake on the pharmacokinetics of organic anions. *Drug Metab Dispos* **39:**1930-1938.

Lave T, Dupin S, Schmitt C, Chou RC, Jaeck D, and Coassolo P (1997) Integration of in vitro data into allometric scaling to predict hepatic metabolic clearance in man: application to 10 extensively metabolized drugs. *J Pharm Sci* **86:**584-590.

Li C and Jiang Y (2012) Analysis of repaglinide enantiomers in pharmaceutical formulations by capillary electrophoresis using 2,6-di-o-methyl-beta-cyclodextrin as a chiral selector. *J Chromatogr Sci* **50:**739-743.

Ménochet K, Kenworthy KE, Houston JB, and Galetin A (2012a) Simultaneous assessment of uptake and metabolism in rat hepatocytes: a comprehensive mechanistic model. *J Pharmacol Exp Ther* **341:**2-15.

Ménochet K, Kenworthy KE, Houston JB, and Galetin A (2012b) Use of Mechanistic Modelling to Assess Inter-Individual Variability and Inter-species Differences in Active Uptake in Human and Rat Hepatocytes. *Drug Metab Dispos* **40:**1744-1756.

Nezasa K, Takao A, Kimura K, Takaichi M, Inazawa K, and Koike M (2002) Pharmacokinetics and disposition of rosuvastatin, a new 3-hydroxy-3-methylglutaryl coenzyme A reductase inhibitor, in rat. *Xenobiotica* **32:**715-727.

Paine SW, Parker AJ, Gardiner P, Webborn PJ, and Riley RJ (2008) Prediction of the pharmacokinetics of atorvastatin, cerivastatin, and indomethacin using kinetic models applied to isolated rat hepatocytes. *Drug Metab Dispos* **36:**1365-1374.

Peters SA (2012) *Physiologically-Based Pharmacokinetic (PBPK) Modeling and Simulations: Principles, Methods, and Applications in the Pharmaceutical Industry*. John Wiley & Sons, Inc.

Poirier A, Lave T, Portmann R, Brun ME, Senner F, Kansy M, Grimm HP, and Funk C (2008) Design, data analysis, and simulation of in vitro drug transport kinetic experiments using a mechanistic in vitro model. *Drug Metab Dispos* **36:**2434-2444.

Rawden HC, Carlile DJ, Tindall A, Hallifax D, Galetin A, Ito K, and Houston JB (2005) Microsomal prediction of in vivo clearance and associated interindividual variability of six benzodiazepines in humans. *Xenobiotica* **35:**603-625.

Sohlenius-Sternbeck AK (2006) Determination of the hepatocellularity number for human, dog, rabbit, rat and mouse livers from protein concentration measurements. *Toxicol In Vitro* **20:**1582-1586.

Szákacs T, Veres Z, and Vereczkey L (2001) In vitro-in vivo correlation of the pharmacokinetics of vinpocetine. *Pol J Pharmacol* **53:**623-628.

Treiber A, Schneiter R, Delahaye S, and Clozel M (2004) Inhibition of organic anion transporting polypeptide-mediated hepatic uptake is the major determinant in the pharmacokinetic interaction between bosentan and cyclosporin A in the rat. *J Pharmacol Exp Ther* **308:**1121-1129.

Watanabe T, Kusuhara H, Maeda K, Kanamaru H, Saito Y, Hu Z, and Sugiyama Y (2010) Investigation of the rate-determining process in the hepatic elimination of HMG-CoA reductase inhibitors in rats and humans. *Drug Metab Dispos* **38:**215-222.

Xiao Q, Tang L, Xu R, Qian W, and Yang J (2015) Physiologically based pharmacokinetics model predicts the lack of inhibition by repaglinide on the metabolism of pioglitazone. *Biopharm Drug Dispos* **36:**603-612.